Proteome-wide and matrisome-specific atlas of the human ovary computes fertility biomarker candidates and open the way for precision oncofertility

Emna Ouni [a], Valerie Nedbal [b], Marta Da Pian [c], Hangbao Cao [d], Kalina T. Haas [e], Alexis Peaucelle [e], Olivier Van Kerk [a], Gaetan Herinckx [f], Etienne Marbaix [g,h], Marie-Madeleine Dolmans [a,h], Timo Tuuri [i], Marjut Otala [i], Christiani A. Amorim [a] and Didier Vertommen [f]

***a* - Pôle de Recherche en Gynécologie,** *Institut de Recherche Expérimentale et Clinique, Université Catholique de Louvain, Avenue Mounier 52, bte B1.52.02, Brussels 1200, Belgium*
***b* - Global Technical Enablement,** *SAS Institute GmbH, Heidelberg 69118, Germany*
***c* - Elsevier B.V.,** *Amsterdam 1043 NX, the Netherland*
***d* - Elsevier Inc.,** *Rockville 20852, USA*
***e* - Institute Jean-Pierre Bourgin,** *INRAE, AgroParisTech, Université Paris-Saclay, Versailles 78000, France*
***f* - PHOS Unit and MASSPROT Platform de Duve Institute,** *Université Catholique de Louvain, Brussels 1200, Belgium*
***g* - Cell Biology Unit,** *de Duve Institute, Université Catholique de Louvain, Brussels 1200, Belgium*
***h* - Gynecology and Andrology Department,** *Cliniques Universitaires Saint-Luc, Brussels 1200, Belgium*
***i* - Department of Obstetrics and Gynecology,** *Helsinki University Hospital, University of Helsinki, Helsinki 00029, Finland*

Corresponding to Christiani A Amorim: *Pôle de Recherche en Gynécologie, Institut de Recherche Expérimentale et Clinique, Université Catholique de Louvain, Avenue Mounier 52, bte B1.52.02, Brussels 1200, Belgium.*
christiani.amorim@uclouvain.be.
https://doi.org/10.1016/j.matbio.2022.03.005

Abstract

Our modern era is witnessing an increasing infertility rate worldwide. Although some of the causes can be attributed to our modern lifestyle (e.g., persistent organic pollutants, late pregnancy), our knowledge of the human ovarian tissue has remained limited and insufficient to reverse the infertility statistics. Indeed, all efforts have been focused on the endocrine and cellular function in support of the cell theory that dates back to the 18th century, while the human ovarian matrisome is still under-described. Hereby, we unveil the extracellular side of the story during different periods of the ovary life, demonstrating that follicle survival and development, and ultimately fertility, would not be possible without its involvement. We examined the human ovarian matrisome and described its remodeling from prepuberty until menopause, creating the first ovarian proteomic codex. Here, we confidently identified and quantified 98 matrisome proteins present in the three ovary groups. Among them, 26 were expressed differently among age groups, delineating a peculiar matrisomal fingerprint at each stage. Such proteins could be potential biomarkers phenotyping ovarian ECM at each age phase of female reproductive life. Beyond proteomics, our study presents a unique approach to understanding the data and depicting the spatiotemporal ECM-intracellular signaling networks and remodeling with age through imaging, advanced text-mining based on natural language processing technology, machine learning, and data sonification. Our findings provide essential context for healthy ovarian physiology, identifying and characterizing disease states, and recapitulating physiological tissues or development *in vitro*. This comprehensive proteomics analysis represents the ovarian proteomic codex and contributes to an improved understanding of the critical roles that ECM plays throughout the ovarian life span.
© 2022 Elsevier B.V. All rights reserved.

Introduction

Before the early 1800s, the 'fibers' of connective tissue were thought to be somehow alive, where life arose by spontaneous generation [1]. Indeed, extracellular matrix (ECM) composed of 'fibers' of different kinds and in various arrangements, known under a variety of other names at that era, preceded the discovery of cells by centuries, even thousands of years [2]. Nevertheless, the fiber theory was later argued and attacked by Rudolf Virchow in the middle 1800s [3] and was finally replaced by the cellular theory, which states that cells arise only from cells (*Omnis cellula e cellula*) [4]. This is a remarkable turnaround from fibers are and make life to cells are life and make fibers. Along with the pursuit of the origins of life, reproduction and how a new individual is generated have long fascinated mankind. At that time, Theodore Schwann proposed that the ovum was also a cell, yet more than 20 years elapsed before Karl Gegenbaur, in 1861, demonstrated convincingly that the ova of all vertebrates are cells. William Harvey's dictum (*Ex ovo omnia*) that all living creatures come from an egg was, therefore, ready to be confirmed more than 200 years after it was conceived [5].

Until today, the ovarian cells and the ovum have remained the center of many research interests, putting the implication of the ECM in reproduction as a secondary matter. Although cells undoubtedly make the ECM, they are, in turn, dependent on it. Indeed, the biological interactions that constitute life - and disease - take place in a continuum throughout cellular and extracellular space [1]. However, our knowledge of the human ovarian ECM is still limited. Most data on human ovarian tissue and its ECM have been obtained through immunohistological staining [6–8] and thus have not comprehensively identified the compositional profile of ECM proteins neither their evolution and remodeling with age or disease. Moreover, the scarcity of healthy human ovarian biopsies has prompted the use of animal models. However, substantial differences between animal and human reproductive systems may question our fundamental understanding of homeostatic ovarian function in our species [9]. Despite these limitations, ECM biology is now starting to gain momentum in reproductive medicine, mainly in the pathological context such as primary ovarian insufficiency, ovarian aging, polycystic ovary syndrome (PCOS), and clinical applications of fertility preservation. Therefore, it is high time we revealed more insights on ECM-cell interactions in the human ovary, integrating all components of the essence of life that have been defined so far: fibers, cells, and ovum.

In this study, we applied our DC-MaP approach [10] and adopted a tailored experimental design of tandem mass tag (TMT) labeling to compare the matrisome of prepubertal, reproductive-age, and menopausal ovarian tissue. The spaciotemporal deposition of matrisome age-biomarkers have been validated with light-sheet microscopy-based-3D imaging, following immunofluorescence and tissue clearing with an ovary-tailored protocol. We used machine learning and statistics to build a neural network that predicts the probability of a specific ovarian tissue matrisome to resemble prepubertal, reproductive-age, or menopausal tissue. We also used Nature Language Processing (NLP) medscan technology for advanced literature text-mining to predict all possible connections between the extra- and intracellular regulators [11] and how gonadotoxic chemotherapeutic agents can also affect key matrisome proteins. Beyond data mining and visualization, this project presents a unique toolbox to understanding the data and depicts the ECM remodeling with age through data sonification. We believe that this technique could help scientists identify ovarian anomalies in proteins more easily by listening to them and catalyze the transition of MS to clinical use.

Our results represent an unprecedented knowledge base in understanding the significant remodeling and alterations occurring in the ovarian matrisome throughout the human life cycle. They also provide a valuable reference for comparative studies between healthy and pathological conditions, as they represent a trustful basis for tissue engineering applications such as the transplantable artificial ovary [12]. We are convinced that these data will pave the way for precision medicine and computed gynecology, and help understand the increasing rate of female infertility, one of the highest global disabilities of our era.

Results

Overview of detected proteins in numbers

We confidently (unique peptides $\geq$ 2; FDR $<$ 1%) identified 120 matrisome proteins, among which 98 proteins were quantified in all samples and included: 16 collagen types; 27 glycoproteins; 8 proteoglycans; 16 ECM-affiliated proteins; 22 ECM regulators, and 9 secreted factors. In addition, 1045 cellular proteins were also confidently detected, including 825 quantified proteins.

Ovarian matrisome remodeling from prepuberty until menopause mirroring ovarian activity at each stage

Thanks to our DC-MaP strategy complemented by 16-plex pro-TMT labeling (Fig. 1), we could confidently detect and quantify 98 matrisome proteins

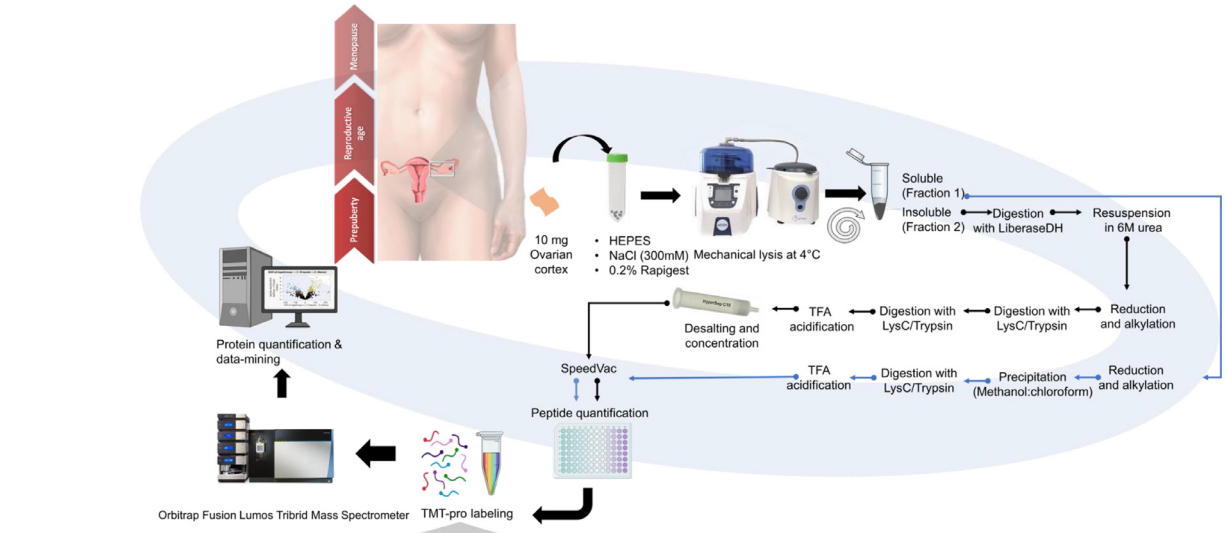

16-plex sample sets	Reporter 1	2	3	4	5	6	7	8	9	10	11	12	13	14	15	16
Set 1	A2	A1	A3	C2	B1	C3	B4	C5	A5	C1	B3	C4	A4	B5	B2	bridge
Set 2	C5	A4	B4	A3	B1	A2	C2	B5	B3	B2	C1	C4	A1	C3	A5	bridge

A1 : fraction 1 (soluble)
A1: fraction 2 (insoluble)

- 3 age groups (A, B, C)
- 5 patients per group = 15 samples (1-15)

Fig. 1. Experimental workflow of quantitative analysis using the DC-MaP fractionation and TMT pro 16-plex isobaric labeling strategy.

within human ovarian tissue over the three investigated groups, which makes it the first dataset of the temporal remodeling of the human ovarian tissue during a woman's life. Interestingly, using one-way ANOVA (FDR$<$0.05), we revealed that 26 matrisome proteins were expressed differently among prepubertal, reproductive-age, and menopausal ovarian tissues and delineated a peculiar matrisomal fingerprint at each age (Fig. 2). Hierarchical clustering enabled the determination of 5 distinct clusters designating upregulated proteins: (i) at prepuberty and downregulated in reproductive age; (ii) at prepuberty and downregulated in menopause; (iii) at reproductive age; (iv) similarly expressed in reproductive and menopausal age and (v) at menopause.

To decipher the main cellular processes where each cluster is implicated, we used gene set enrichment analysis (GSEA) with a $p \leq 0.05$. Selected biological processes were annotated for each cluster. Thus, we were able to spot enriched cellular processes in an age-related manner.

Prepuberty

Prepubertal ovarian tissue has the highest number of unique matrisome proteins reaching 13 upregulated biomarkers. Although collagen type VI is revealed to be the dominant collagen type in human ovarian tissue at all ages, its highest levels were detected during prepuberty (Fig. 2.A). At this stage, the enriched cellular processes describe the ovarian ECM as under fundamental remodeling and construction (Fig. 2.B). Indeed, proteins implicated in elastic fiber assembly (FBLN5 and POSTN) and ECM fiber polymerization (TNXB) were overexpressed. Moreover, proteins involved particularly in basement membrane assembly (COL4 and NID1) and repair (ANXA7) were significantly highly abundant compared to adult ovaries.

Beyond matrisome protein structural role, fundamental cellular processes related to follicular atresia and quiescence could be linked to prepubertal matrisome hallmarks (Fig. 2.B). On one side, primordial follicles (dormant follicles) are dominant during prepuberty and present original features of quiescence and long survival. This could be in part regulated by COL14A1, which promotes quiescence in corroboration with anti-apoptotic matrisome proteins, such as HRNR [13]. On the other side, the infant ovary is also characterized by an increasing follicle loss preceding puberty, which could be assigned for high expression of pro-apoptotic proteins [14]: OGN and TGFBI.

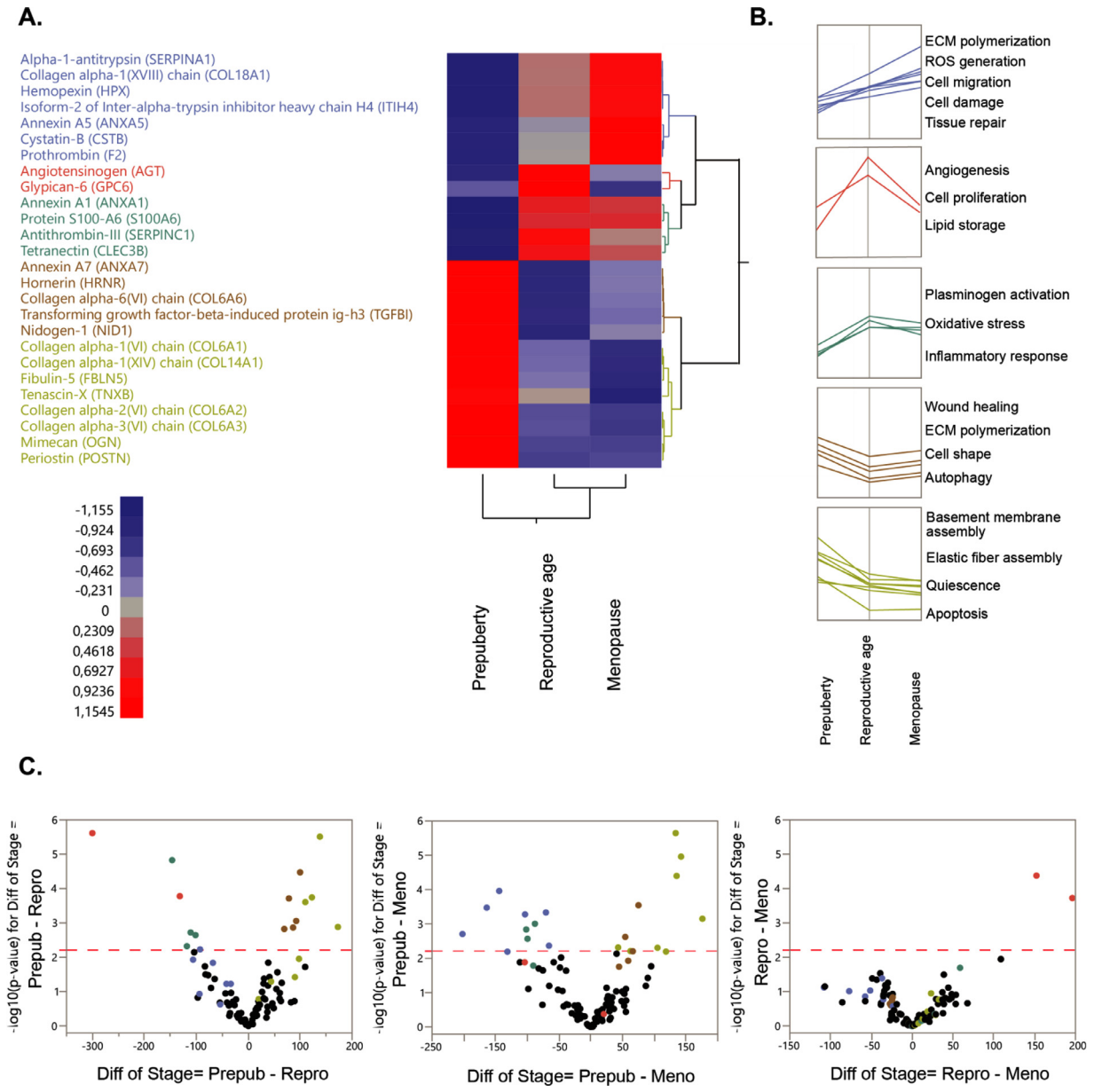

Fig. 2. Ovarian matrisome remodeling throughout life. A. Hierarchical clustering of 26 matrisome proteins, with significantly different expression levels between prepubertal, reproductive-age and menopausal ovaries (one-way ANOVA, FDR$<$0.05). Five clusters of these proteins are depicted based on different intensity profiles. B. To decipher main cellular processes where each cluster is implicated, we used GSEA with a p$\leq$0.05. Parallel plots highlight the protein expression tendency throughout age in each cluster. C. Volcano plots showing pairwise comparisons of protein expression levels between various stages. Points above horizontal dashed lines represent significantly altered proteins (two-sided t test, p$<$0.05, p values were adjusted by Benjamini–Hochberg correction for multiple comparisons). Heatmap of replicates can be found on Supp Fig.3.

Reproductive age

At reproductive age, all matrisomal hallmarks of prepuberty have declined, and only two proteins appear to be exceptionally highly expressed in this age group: AGT and GPC6 (Fig. 2.A,C). AGT has been enriched in the renin angiotensinogen system (RAS), which is presumed to regulate oocyte maturation and quality, promote angiogenesis and lipid storage [15,16]. GPC6 is a positive regulator of cell proliferation, a paramount process for follicle development [17,18].

Menopause

Seven matrisomal proteins weakly expressed during prepuberty, increase progressively at reproductive age, and reach their peak upon menopause and have been enriched in several cell processes (Fig. 2.A,B).

The only collagen type upregulated at menopause is non-fibrillar, COL18A1. This endostatin-producing collagen has been known as an inhibitor of endothelial cell migration and angiogenesis [19,20]. Among menopause matrisomal biomarkers, we could find upregulated proteins responsible for (Fig. 2.B): ECM production, polymerization, and fibrosis (ANXA5, F2, ITIH4, and SERPINA1). Interestingly, almost the same proteins active in fibrosis play an important role in promoting cell survival (ANXA5, F2, HPX, SERPINA1), preventing cell damage (HPX, SERPINA1), inhibiting reactive oxygen species (ROS) generation (HPX, SERPINA1, and CSTB), and are implicated in hemolysis inhibition (ANXA5) and protection against heme toxicity (HPX), as depicted by GSEA. In conjunction with their cytoprotective effects, ANXA5, SERPINA1, and F2 are also associated with senescence [21−23].

Although we would expect a large panel of differences compared to reproductive-age ovarian tissue (the gold standard of fertility), hierarchical clustering of quantified ECM proteins revealed common matrisomal features (Fig. 2). While it was not surprising to find a higher plasminogen activation in reproductive tissue since it is one of the major ECM degradation and remodeling processes during the ovarian cycle enabling ovulation [24], we noticed that plasminogen stimulator, CLEC3B [25], remains highly expressed in the human ovary even after menopause, concomitantly with the expression of the anti-inflammatory and anti-oxidative ECM proteins ANXA1 and SERPINC1 [26,27]. This may mirror the presence of a peculiar inflammation process at menopause even in the absence of ovulation occurring during ovarian aging and further highlights the plethora of roles that matrisome proteins may play.

Change in collagen hydroxylation level as one of ovarian aging hallmarks

Proline hydroxylation of all quantified proteins with our DC-Map TMT-based workflow has been screened (Fig. 3.A, Supp Table 1). In the matrisome, we found 13 collagens and one proteoglycan (lumican) differently hydroxylated between age groups at 253 locations (peptide sequences). Proline hydroxylation may regulate the flexibility of collagen molecules and make functional sites available for interacting proteins and receptors [28]. With the value of this post-translational modification in mind, our results revealed that menopausal ovarian collagen is the least hydroxylated compared to younger ones, which may reflect an abnormal and unstable collagen assembly with limited interaction with cell receptors and other matrisome proteins at such stage. By contrast, reproductive-age ovaries are characterized by the highest hydroxylation of fibril forming collagen such as COL1A1, COL1A2, COL5A1, and COL5A2. Among matrisomal hallmarks of prepuberty, we found the highest hydroxylation of non-fibrillar COL6 and COL14 at this group, with a remarkable hydroxylation of the fibrillar COL3 (Fig. 3.A).

In addition to collagen hydroxylation, lumican was also hydroxylated. Lumican is a small leucine-rich proteoglycan that colocalizes with fibrillar collagen and regulates the assembly and diameter of collagen fibers [29]. Despite the presence of lumican and other fibrillar collagen types, namely type I, II, III, and V at equivalent levels in ovarian tissue at all stages (Fig. 2), the depicted differences in their hydroxylation may impact ECM architecture [30] and suggest a possible collagen synthesis by different cell populations within the studied groups [31].

Machine learning (neural network) as a potential predictive method of ovarian tissue biological age and fertility potency

Our collected proteomic data on ovarian matrisome temporal remodeling from prepuberty til menopause were used to build a neural network. The neural network reveals the synergy of matrisome proteins and their expression level interdependence. As it also predicts the probability of a specific ovarian tissue matrisome to resemble to prepubertal, reproductive-age, or menopausal tissue.

Ordinary least-squares gave us a model with an R-square value of 0.96 and a small RMSE=0.20 on the testing set, which proves the goodness of fit of our model. Based on the TanH hyperbolic tangent function, the neural network relied on three nodes. The results of our model can be seen (.html format) or interactively tested to evaluate different possible theoretical ovarian profiles (e.g., pathological conditions) by downloading the source data on (.jrp format): https://data.mendeley.com/datasets/22t56fbd6t/draft?a=4b98519d-dfb4−4fe0-a1b0-b4e75b360be6and opening the jrp file using JMP software (accessible demo): https://www.jmp.com/en_us/download-jmp-free-trial.html.

We noticed that variations in GPC6, ITIH4, ANXA5, or TNXB levels lead to high variability in the response, which reveals their important effect on the model and eventually on the rest of ovarian matrisome and encourages their deeper investigation. For instance, by decreasing the level of GPC6 by one fold change the profil ressembles more to a

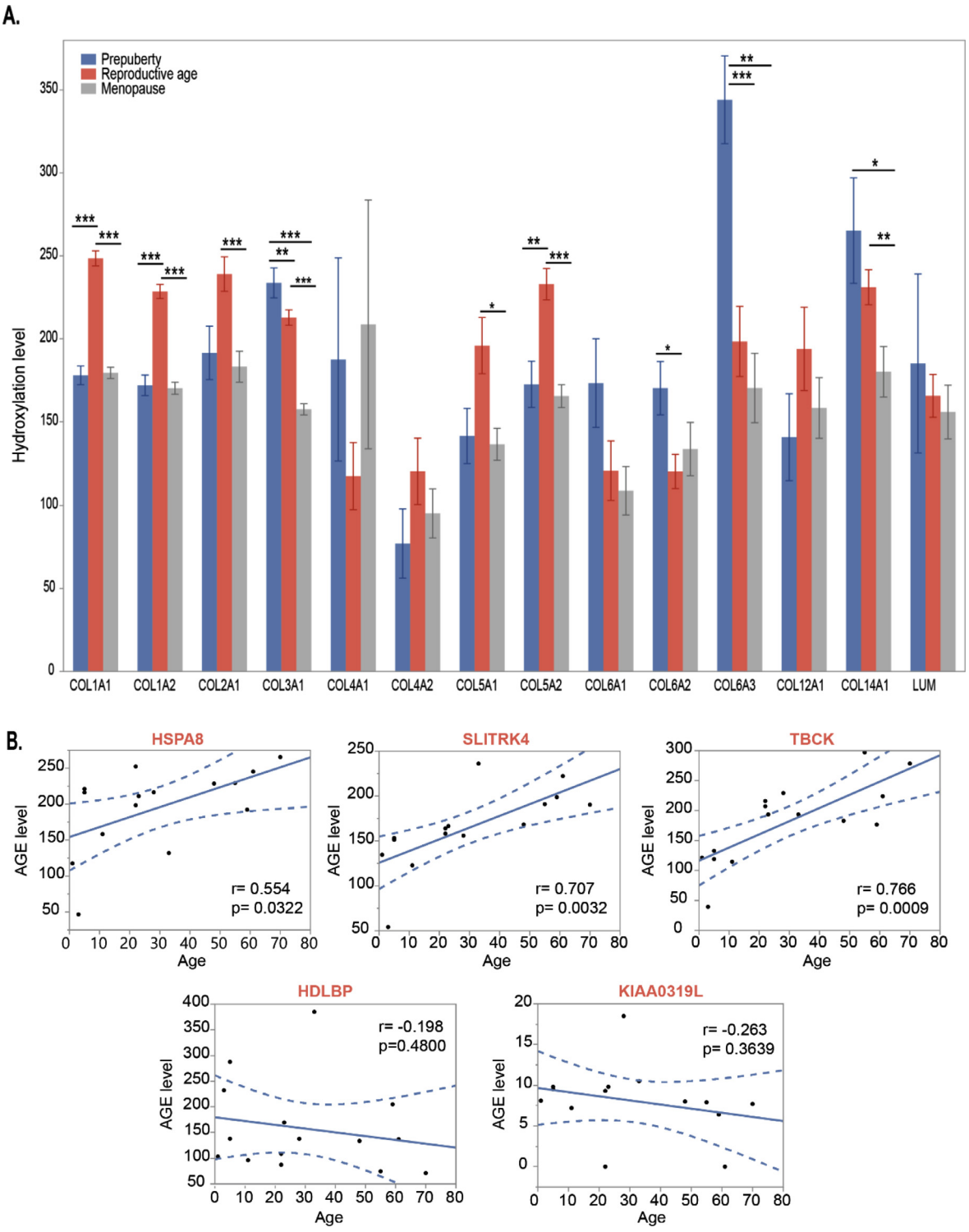

Fig. 3. Post-translational modification at the extra-and intracellular compartments.

A. Hydroxylation intensities. Histogram represents means and standard errors. B. Advanced glycation end products (AGEs) intensities according to age. Pearson's correlation was used to study age-AGEs relationship. Steel-Dwass method was used to compare intensities between groups (*$p<0.05$, **$p<0.01$, ***$p<0.001$). Full statistical interactive reports with details on each modification position at every data point can be found on (.html format): https://data.mendeley.com/datasets/22t56fbd6t/draft?a=4b98519d-dfb4−4fe0-a1b0-b4e75b360be6.

menopausal matrisome rather than a reproductive age one which suggests the potential role of GPC6 as a fertility biomarker candidate.

The model has been built based on gathered data developed with our specific pipeline and thus, for the moment, only reflects ovarian matrisome detected with these experimental conditions. However, we foresee in the future the collection of larger data from several proteomic platforms that can enrich ours and overcome technical variabilities, which can benefit medical diagnostics and data analysis. Indeed, neural networks can tolerate up to 15% error and still produce a robust result [32]. In some cases, introducing noise to the dataset can actually improve the performance of the network [32].

Intracellular proteome temporal dynamics and their homeostatic functions at each stage with unique cytoprotective activity during menopause

Prepuberty

Among the 825 confidently detected cellular proteins, around 182 ones are particularly upregulated during prepuberty (FDR$<$0.05) and were enriched in 3 main biological processes: mitochondrial damage, immune chemotaxis, aberrant RNA clearing (Fig. 4). Excessive follicule atresia in the ovary and significant loss of follicular reserve, especially during prepuberty [33], can be attributed to mitochondria, whether by promotion of mitochondrial damage [34] by the release of cytochrome C (PARP1, MIF, VDAC1, SLC25A4), mitochondrion autophagy (PPID, PHB2) or mitochondrion fission (UTRN, RALA, CS). All of which leads to cell death. An important activity of immune cell recruitment also appears to occur during prepuberty, namely, under the control of S100A8, S100A9, and PTGDR implicated in neutrophil recruitment and PPIB and MIF regulating macrophage migration and activation. Although immune cell implication in ovarian function has already been described [35], our data further outline their possible involvement in releasing pivotal cytokines and growth factors. These proteins are necessary for the development of the ovary's functional aspects and release of chemokines that attract and activate additional monocytes and neutrophils into the ovary from circulation and secrete an array of proteases that degrade the ECM as well as release/alter ECM- or membrane-bound proteins [36] (Fig. 4).

The central dogma of molecular biology posits that the genetic information encoded in DNA is transcribed into RNA and then translated into protein. During this process, regulation of RNA splicing represents a critical step of gene expression which directly impacts the translation of that genetic information into protein. In prepubertal tissue, we have detected proteins that prevent RNA splicing and ensure homeostasis, such as DDX1, RPS3, RPL30, PTBP1, and RPS14 (Fig. 4). Nonsense-mediated mRNA decay, which can be defined by the loss of mRNAs carrying premature stop codons, is a process by which cells recognize and degrade nonsense mRNAs to prevent possibly toxic effects of truncated peptides (Fig. 4). This homeostatic process in prepubertal ovaries is promoted by the upregulation of SRSF1, SRSF2, and GPX1. Since nonsense mRNA can lead to ovarian insufficiency in adult life [37], it seems that nonsense-mediated mRNA catabolism proteins may play a fundamental role in the faith of ovarian reproductive potency during adult life.

Reproductive age

At reproductive age, nonsense mRNA decay continues through upregulated HNRNPL and TPI1, which complements the previously described prevention of the consequences of truncated peptides (Fig. 4). An additional cellular process related to the prevention of abnormal protein synthesis is enriched in reproductive age ovaries. It consists of the inhibition of endoplasmic reticulum stress, which occurs when proteins are not correctly folded or conformed (misfolded protein). Consequently, through the upregulation of P4HB [38], CALU [39,40], GPI [41], and CALR [42], reproductive-age ovaries are able to limit endoplasmic stress that interferes with the normal physiological functions of cells. Among the 41 cellular proteins that are particularly upregulated at reproductive age, we found anti-senescence proteins, namely: TPI1, HNRNPD, ENO1, and FSCN1 (Fig. 4). While senescence could hamper fertility, follicular quiescence could also interfere with the growth and release of eggs from the ovaries (ovulation), such as the case for PCOS patients [18]. Both processes can lead to infertility, and thus through identifying their regulators in healthy reproductive-age ovaries, we can better target their disfunction in pathological conditions. One of the targets of the recent therapies under development for PCOS patients is actin, since its polymerization reestablishes follicle activation [43]. Bearing this in mind, we found in healthy reproductive ovarian tissue proteins promoting actin polymerization, namely: TPM1, TPM2 and PGK1, which could be further investigated in the context of PCOS and present promising therapeutical targets.

Menopause

Among the 45 upregulated cellular proteins in menopausal ovarian tissue, two have been related to promoting DNA fragmentation: PRF1 and IAPP. Despite expected aging hallmarks such as mitochondrial damage (DBI) and ROS generation (AOX1, PRF1, and CLIC1), menopausal ovaries appear to have their

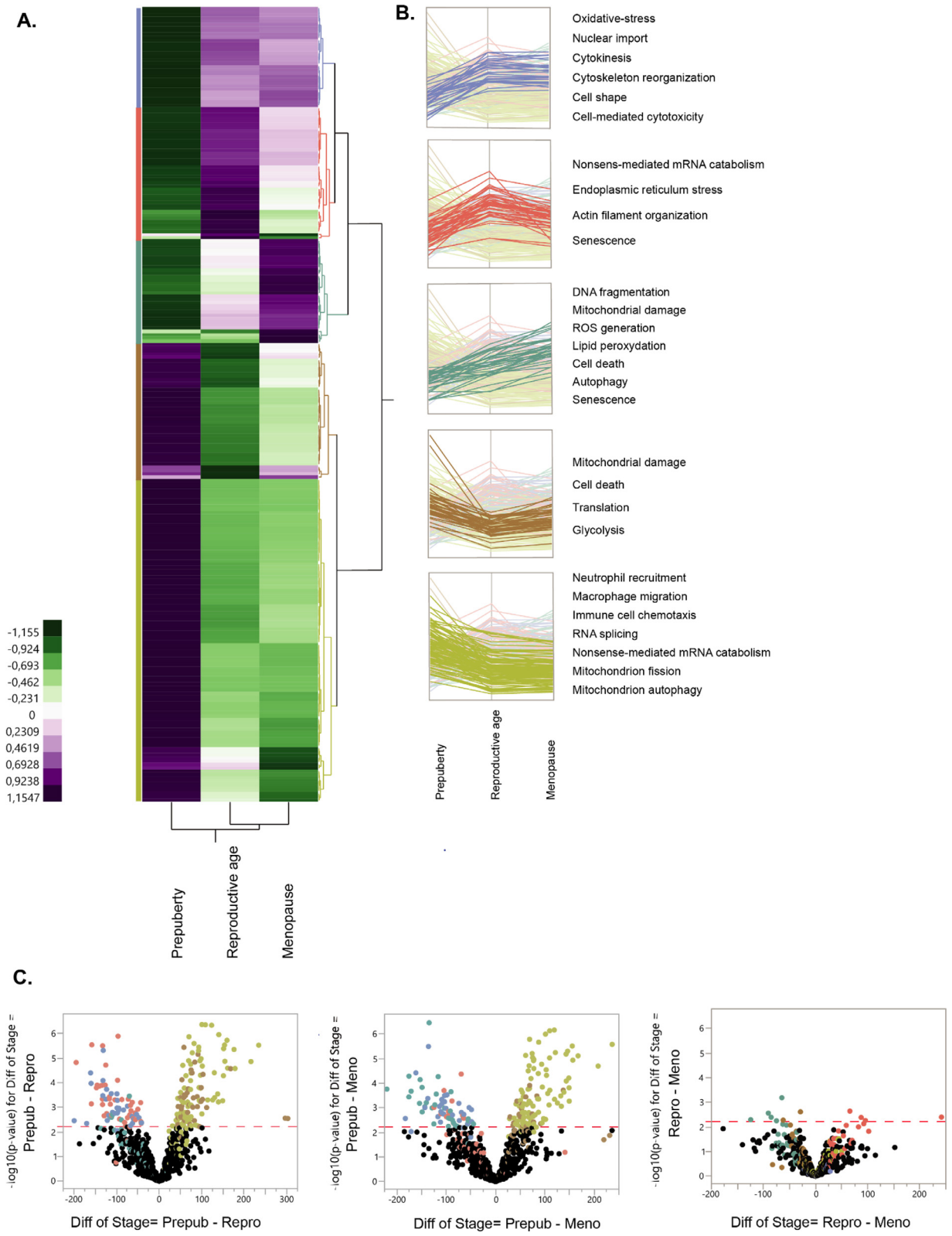

Fig. 4. Cellular protein shift with age. A. Hierarchical clustering of 246 cellular proteins, with significantly different expression levels between prepubertal, reproductive-age and menopausal ovaries (one-way ANOVA, FDR<0.05).

Five clusters of these proteins are depicted based on different intensity profiles. B. To decipher main cellular processes where each cluster is implicated, we used GSEA with a $p \leq 0.05$. Parallel plots highlight the protein expression tendency

own anti-oxidative stress shield controlled by PRDX6, preventing lipid peroxidation and DNA damage and PKM, DBI, GAPDH, and SLPI limiting ROS production (Fig. 4). Other proteins upregulated at menopause play an important cytoprotective role (mechanoprotection, neuroprotection), such as FLNA, YWHAQ, CSRP1, AFM, and GSTM2. On the other hand, autophagy is halted by the overexpression of TSPO and DAP [44,45]. Limitation of both cell death and autophagy processes may reinforce cell senescence in aging ovarian tissue. Indeed, senescence is also another enriched cell process promoted by upregulation of DBI and TSPO but also by ZYX, ARID4A, RNASEH1, RBP1, and PRDX6 (Fig. 4).

Despite significant differences between menopausal and reproductive-age ovarian tissues, both groups share common expression levels of 37 cellular proteins, downregulated in prepubertal ovaries, among which a high number of anti-oxidative stress proteins, such as ADH5, PEBP1, TALDO1, PSME1, MPST, and DDT, which complement the unique anti-oxidative proteins only upregulated during menopause as mentioned above (Fig. 4). The enriched cellular processes reflect a high cellular activity at menopause with common regulators with reproductive age tissue, such as nuclear import responsible for transporting transcriptional factors toward the nucleus (YWHAB, YWHAZ, YBX1, CFL1, and DCTN2) and cytokinesis (ARHGDIA, CRK, and DDT), which are operating via focal adhesion and cytoskeleton reorganization and influencing, consequently, cell shape, spreading and mechanosensing (RDX, CRKL, and DCTN2).

Among the shared enriched mechanisms between reproductive-age and menopausal ovaries, we also detected common promoters of cell-mediated cytotoxicity, which is a crucial process responsible for the host immune defense against pathogens localized within cells [46]. In the context of the human ovary, many theories have related the immune system to follicle selection, degeneration of large follicles, and ovulation [47]. These events usually are only present at the reproductive age ovary due to follicle reserve presence. However, the pro-cell-mediated cytotoxicity proteins shared with reproductive-age ovaries, TTR, EIF5A, CUTA, and B2M, might suggest their residual action even after menopause.

Advanced glycation end products (AGEs) only detected at the cellular level

Advanced glycation end products (AGEs) are heterogeneous products formed by the non-enzymatic reaction of proteins withreducing sugars [48] and have been associated with aging.

AGE is also considered as one of collagen post-transcriptional modifications that increase with age, inducing higher crosslinking and thus stiffness of collagen structures [49], which is a biomechanical hallmark of aging human ovarian tissue [50]. Nevertheless, in our results AGE were only identified in cellular proteins, namely: HDLBP, HSPA8, KIAA0319L, SLITRK4, and

TBCK, over five distinct sites with variable levels between age groups, despite undetected significant differences in these protein expressions (Fig. 3.B, Supp Table 1). High AGE serum levels have been lately established to diagnose diminished fertility [51] and have been associated with infertility-related diseases [51]. While our data disclose a significant positive correlation between age and AGE-tissue levels at TBCK (r= 0.766; p=0.0009), SLITRK4 (r=0.707; p=0.00032) and HSPA8 (r=0.554; p=0.0322), we also found an age-independent variation in AGE at HDLBP (r=-0.198; p=0.4800) and KIAA0319L (r=-0.317; p=0.2489). Thus our results reveal specifically potential targets affected by AGE during aging, which complements the depicted ovarian phenotype during menopause and may prompt a more precise diagnosis of infertility and premature ovarian aging.

Matrisome biomarkers interaction with mTOR and Hippo pathways

We relied on pathway studio and its Nature Language Processing (NLP) technology to study all possible bidirectional regulation occurring between each of the 26 matrisome biomarkers and members of Hippo or mammalian target of rapamycin (mTOR) signaling pathways. This was necessary to understand the possible interaction of ovarian matrisome biomarkers with these key signaling pathways related to fertility and follicle activation and development. All connections were manually supervised and curated to select the most relevant relationships between the matrisome and cellular proteins.

The mTOR signaling, a regulator of cell growth and proliferation, is a crucial mediator of primordial follicle activation via the Akt pathway in mice [52–55]. Activated Akt works upstream of mTORC1 and promotes mTORC1 phosphorylation leading to the suppression of FOXO3 nuclear transcription, responsible for follicle activation. MAPK3/1 signaling also participates in primordial follicle activation through downstream mTORC1-KITL.

throughout age in each cluster. C. Volcano plots showing pairwise comparisons of protein expression levels between various stages. Points above horizontal dashed lines represent significantly altered proteins (two-sided t test, $p<0.05$, p values were adjusted by Benjamini–Hochberg correction for multiple comparisons). Heatmap of replicates can be found on Supp Fig.3.

While these findings do not consider the implication of ovarian ECM, there is one study that bridges ECM to follicle activation signaling through demonstrating that fragmentation of mouse ovaries promotes follicle growth [43]. This effect was correlated with Hippo pathway disruption due to increased actin polymerization (conversion of G-Actin to F-Actin), which results in accumulation of yes-associated protein (YAP) in the nucleus [43]. The transcription factor YAP upregulates the expression of CCN growth factors that modulate follicle growth and oocyte maturation [43]. Nevertheless, until our study, the Hippo pathway was not linked directly to matrisome proteins. Our analytical method revealed all the possible interactions between matrisomal biomarkers at each age and their targets at both Hippo and mTOR pathways.

Hippo pathway

In the prepubertal ovarian tissue, we found inhibitors of Hippo pathway (COL6A3 and FBLN5) at the matrisome level, possibly implicated in follicle activation, which stimulates YAP activation (Table 2, Supp Fig. 1, Supp Table 2). Interestingly, most ovarian matrisome proteins appear to interact with the Hippo pathway through E-cadherin, a major regulator of the Wnt/β-catenin signaling pathway. For instance, upregulated TGFBI and OGN during prepuberty lead to downregulation of E-cadherin and β-catenin stabilization and its nuclear localization, which stimulate Wnt/β-catenin activity. Knowing that Wnt/β-catenin has been previously described as hampering follicle activation and development [56,57], TGFBI and OGN can be consequently considered as potential inhibitors of follicle activation (Table 2, Supp Fig. 1, Supp Table 2).

Upon puberty, upregulation of GPC6 declines Wnt/β-catenin signaling, promoting follicle activation, while an upregulated AGT activates the renin-angiotensin system (RAS) that has been related to oocyte maturation and its quality regulation [58]. Similarly, high levels of S100A6 and ANXA1 in reproductive-age and menopausal patients compared to prepubertal ones are linked to alterations in tight junction assembly and E-cadherin stability, which may weaken the interaction between E-cadherin and β-catenin at the membrane and lead to the translocation of the latter to the nucleus, consequently activating the repressive effect of Wnt/β-catenin signaling on follicles (Table 2, Supp Fig. 1, Supp Table 2).

In humans, this resting state could last for decades, and some follicles, although scarce, may stay in a dormant state even after menopause. Although upregulation of F2 can promote TAZ activation and consequently follicle recruitment, we noticed that SERPINA1 upregulation also alters tight junctions and E-cadherin as it activates PP2A. PP2A, as one of the most complex Ser/Thr phosphatases (Table 2, Supp Fig. 1, Supp Table 2), was demonstrated to have promiscuous activity resulting in dephosphorylation of proteins involved in a diverse range of biological processes such as cell cycle progression and cell death [59]. Since PP2A acts as an oncogenic or tumor suppressor, depending on its regulatory subunits compositionand substrate, it is hard to predict whether the menopausal matrisome may have precursors of follicle activation.

mTOR pathway

During prepuberty, several matrisomal biomarkers (COL6A1, POSTN, and FBLN5) interact with the mTOR signaling pathway and activate Akt and potentially participate in follicle activation (Table 2, Supp Fig. 2, Supp Table 2). In contrast, the interaction between OGN and mTOR signaling further proves that OGN is a negative regulator of follicle activation. Indeed, OGN negatively regulates Akt activity and blocks cytoskeletal remodeling, limiting the formation of F-actin, one of the hallmarks of follicle activation [43].

Upon puberty, mTOR activity is levitated under the overexpression of AGT. Common highly expressed ECM proteins between reproductive-age and menopausal patients such as S100A6 and ANXA1 appear to regulate follicle activation through pro and repressive actions by phosphorylation of MAPK, Akt, and FOXO3, and stimulation of actin-bundling on one side and activation of p53 (upstream repressor of mTOR) and downregulation of PI3K phosphorylation on the other (Table 2, Supp Fig. 2, Supp Table 2).

During menopause, p53 is also upregulated by ANXA5. Nevertheless, its action is restrained by COL18A1 [20]. Another mTOR promoter during menopause is F2 which also activates its downstream target RPS6KB1 (p70) (Table 2, Supp Fig. 2, Supp Table 2).

Clearly, at each age, the human ovary has its intertwined processes for pro and anti-follicle activation, orchestrating ovarian homeostasis. Although the current results open a new world of opportunities for future investigations and possible clinical targets, experimental validation of the discussed processes will be paramount to decode activation of human ovarian follicles.

Localization and 3D distribution of matrisome biomarkers

To valildate the trends in the 26 ECM biomarker-expressions from the MS study and identify their 3D distribution and localization in the human ovarian tissue from prepuberty until menopause, we conducted immunofluorescence and tissue clearing with an ovary-tailored protocol, followed by light-sheet microscopy acquisition (Fig. 5). The 3D observations

have revealed an important heterogeneity in protein deposition within the same tissue (ANXA1, HPX) and between age groups (COL6A6). We noticed marked architectural remodeling in some ECM biomarkers (COL6A3, COL18A1, F2, ITIH4) and localization shifts (CSTB). Some proteins have been exclusively localized during prepuberty at the follicle level and appear to be expressed by oocyte or granulosa cells (AGT, SERPINC1, ANXA7), which delineate a local matrisomal homeostasis at the follicle periphery.

Overall, qualitatively, the immunofluorescence staining correlates well with and validates the MS data and further predicts possible ultrastructural changes in the 26 biomarkers with age that might reach protein function.

Discussion

Due to the difficulty in obtaining human ovarian tissue, it has been challenging to determine the human ovarian cortex proteomics. Moreover, the fibrous nature of human ovarian ECM makes the pursuit of reliable proteomic characterization strewn with obstacles [10]. Thanks to our DC-MaP protocol for TMT-based matrisome proteomics and our adopted reproducible workflow for analyzing extracted fractions, we could capture the most whole picture of intra- and extracellular proteins [10] (reproducibility of samples within each group is highlighted by pairwise Pearson's correlation analysis in Supp Fig. 3). Here, we present the first proteome-wide and matrisome-specific analysis of the human ovarian tissue at prepubertal, reproductive, and menopausal stages, providing unprecedented insights into the mechanisms by which human ovaries develop, reach reproductive competence, and age in normal conditions.

Among the main discoveries of our study is the dominant collagen type in human ovarian tissue at all ages, COL6 (COL6A1, COL6A2, COL6A3, and COL6A6 identified respectively with 28, 22, 7, and 3

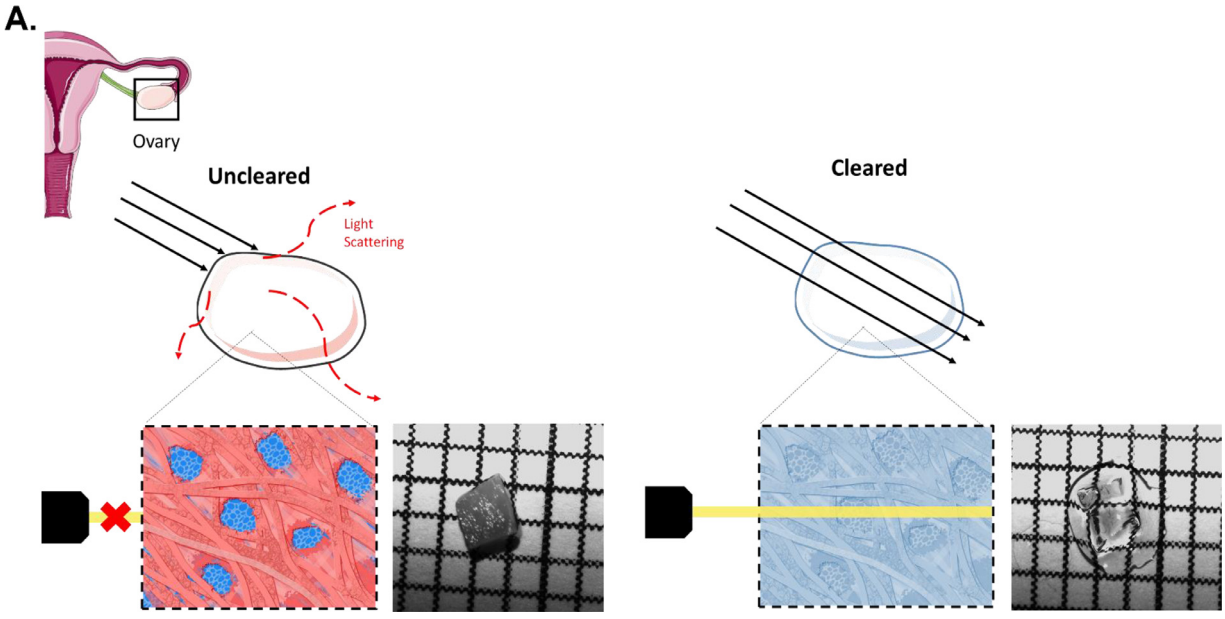

Fig. 5. 3D visualization of ECM biomarkers through cleared ovarian tissues. A. The need for volumetric imaging of ovarian tissue is related to the inherent three-dimensional structure of its cells and ECM. But even with the advent of optical sectioning, this has remained a challenge when it comes to imaging thick tissues. Tissue opacity undermines sharp images and represents an impediment for volumetric observations. This inherent opacity is caused by light scattering. Light rays that should travel in straight lines are deviated many times as light is reflected off of molecules, membranes, organelles, and cells in the tissue. Therefore we used our tissue clearing method to assure that there is a high uniform density of scatterers so that lateral scattering is minimal and that all wavelengths of light pass 'through' the tissue and enable the observation of fluorescent targets in their 3D native structure. B. Captures of the 26 matrisomal biomarkers that have been validated by immunofluorescence and 3D imaging of cleared labeled tissues under lightsheet microscopy at 20X magnification with a digital zoom between 0.7 and 1.5. 3D visualization can be accessed by scanning the corresponding QR code. Qualitative trends in protein levels corroborate MS data. All used antibodies have been validated priorly with 3, 3′-diaminobenzidine immunohistochemical staining (Supp Fig. 4). Proteins of interest were revealed with anti-mouse Ig (red) and anti-rabbit Ig secondary antibodies (green). Hoechst (blue) was used for nuclear staining (Table 1). On the right panel, box plots illustrate the quantification results of matrisomal biomarkers based on image analysis. Green lines define the average value per group. Blue lines connect the means. All paired comparisons were conducted with one way-ANOVA (post hoc: Tukey), different letters stand for statistical significance ($p<0.01$).

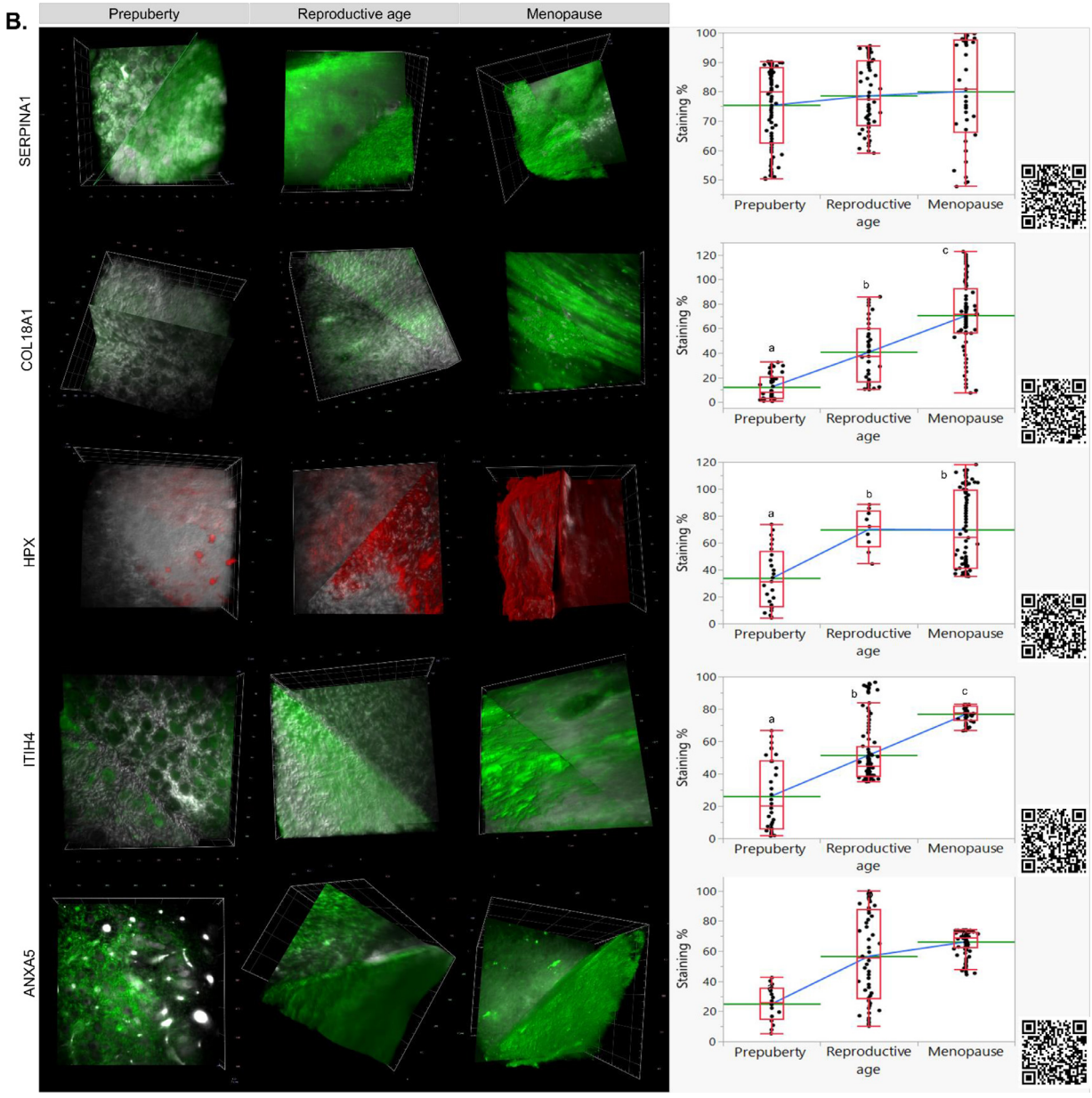

Fig. 5 Continued.

unique peptides), which confirms our previous label-free proteomic study of pre-menopausal ovarian tissue [60] and corrects an ancient thought, reporting that collagen type I was the dominant collagen type in the human ovarian cortex [61,62] and led to several related research using COL1A1 as a scaffold for 3D culture of ovarian follicles and cells [63–67]. COL6 is an unusual member of the collagen family and has been studied in the past few years within the context of an extensive wide range of tissues. The distinctive feature of this protein is its unique supramolecular assembly, which is driven by a multi-step process that leads to the formation of the characteristic beaded microfilaments network in the ECM [68]. COL6 exerts different roles in tissues, spanning from mechanical roles, typical of collagen components of the ECM, to more specific cytoprotective functions (mechanoprotection from compressive forces), including apoptosis and oxidative damage inhibition, cell differentiation, and autophagic machinery regulation [69,70]. COL6 also has bridging and anchoring roles, facilitated through interactions with a wide variety of other ECM proteins, including other collagens, proteoglycans,

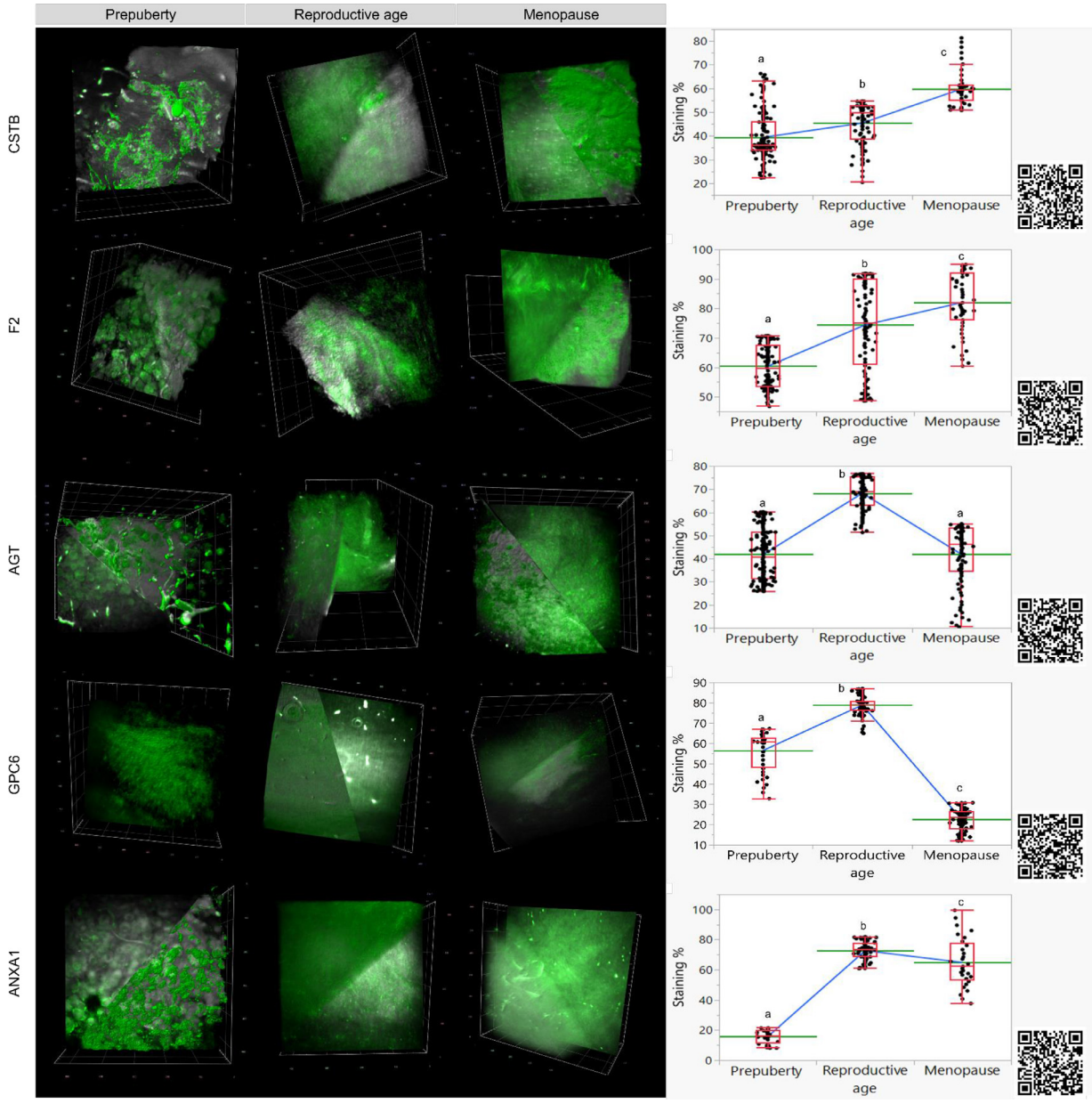

Fig. 5 Continued.

fibronectin, and microfibril-associated proteins. Moreover, COL6 can bind to a range of cell surface receptors including integrins $\alpha1\beta1$, $\alpha2\beta1$, $\alpha3\beta1$, $\alpha10\beta1$, and $\alpha v\beta1$ [69] and thus regulate cell-ECM communication and may represent a communication platform between ovarian follicles and cells. Our temporal follow-up of ovarian matrisome remodeling revealed COL6 as one of the matrisomal fingerprints of prepubertal ovarian tissue, where it is upregulated in synergy with autocrine and paracrine signaling accompanying prepubertal gonadal development. During prepuberty, the human ovarian tissue seems under high elastic structuration and remodeling by FBLN5, POSTN, TNXB, preparing the ovary for its later stages. While COL14A1, HRNR, NID1, and COL6 participate in ovarian follicle dormancy, high expression of OGN, POSTN, and TGFBI stimulate atresia. Both events are characteristic of prepubertal ovaries: while follicle dormancy preserves the ovarian reserve for reproductive-age life, follicle atresia might be a selective process for keeping the most competent follicles [71]. In addition, as we suggested before [72], prepubertal matrisome seems non-permissive to follicle activation from

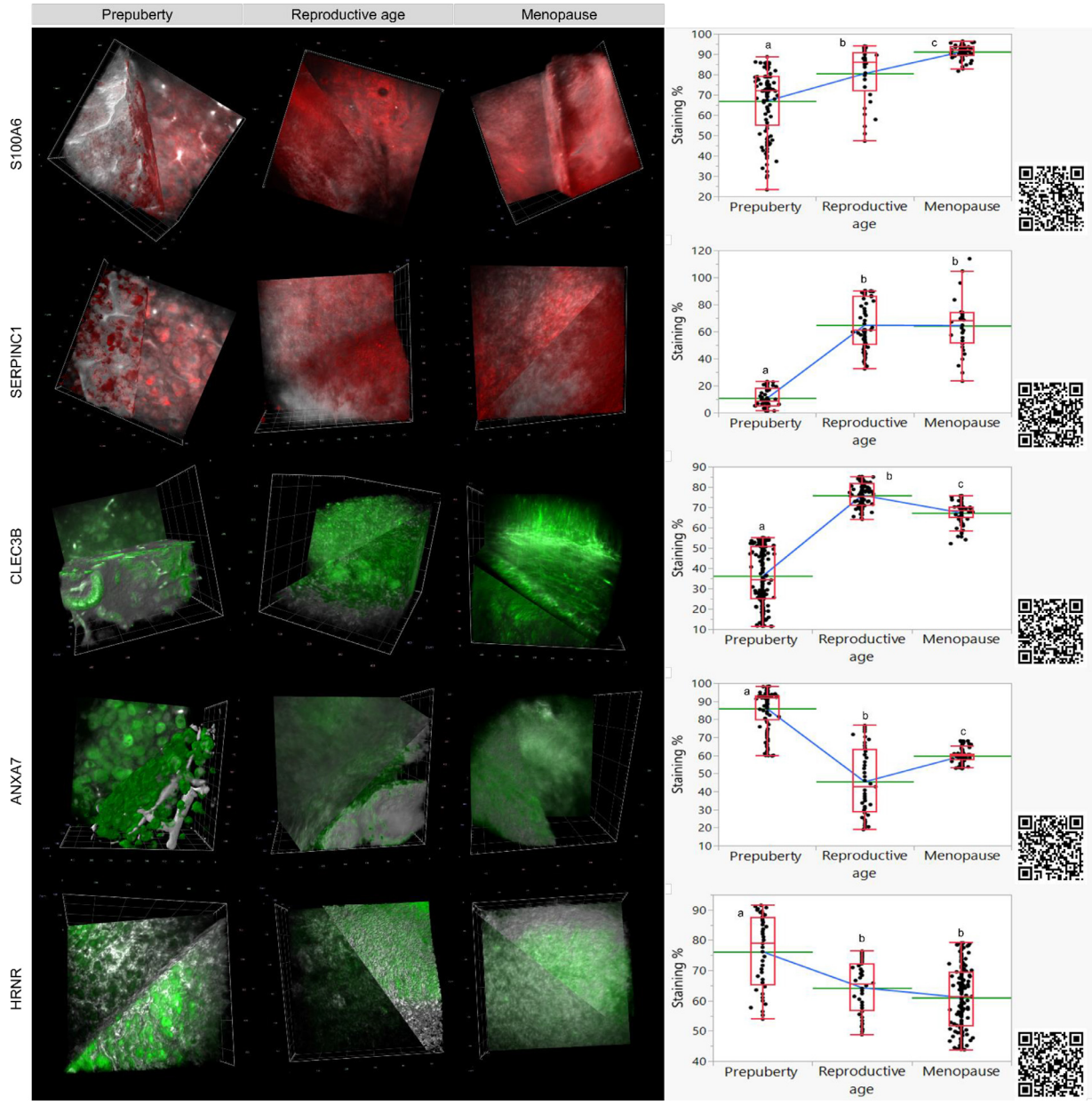

Fig. 5 Continued.

biochemical and mechanical perspectives. At the intracellular level, highly expressed proteins distinguishing the prepubertal ovaries from their age counterparts highlight an intense regulatory process for the elimination of abnormal cells through mitochondrial damage (PARP1, MIF, VDAC1, SLC25A4, and UTRN) and clearing of nonsense mRNA decay (DDX1, RPS3, RPL30, PTBP1, and RPS14).

Upon puberty, only two ECM proteins separate reproductive-age ovaries from infant and menopausal counterparts: AGT and GPC6. AGT is a member of RAS signaling, which regulates oocyte maturation and quality and participates in critical physiological events during ovulation and luteinization [58]. Its production is strongly influenced by estrogens [73], highly secreted by growing follicles at reproductive age. Naturally, deregulation in AGT expression might trigger pathological conditions. Indeed, while AGT deficiency is associated with a decreased fertility [74], RAS enhanced activity is associated with PCOS [75].

The second matrisomal fertility biomarker is the glycoprotein GPC6, a regulator of heparin-binding growth factors such as FGFs, BMPs, Wnts, Hhs,

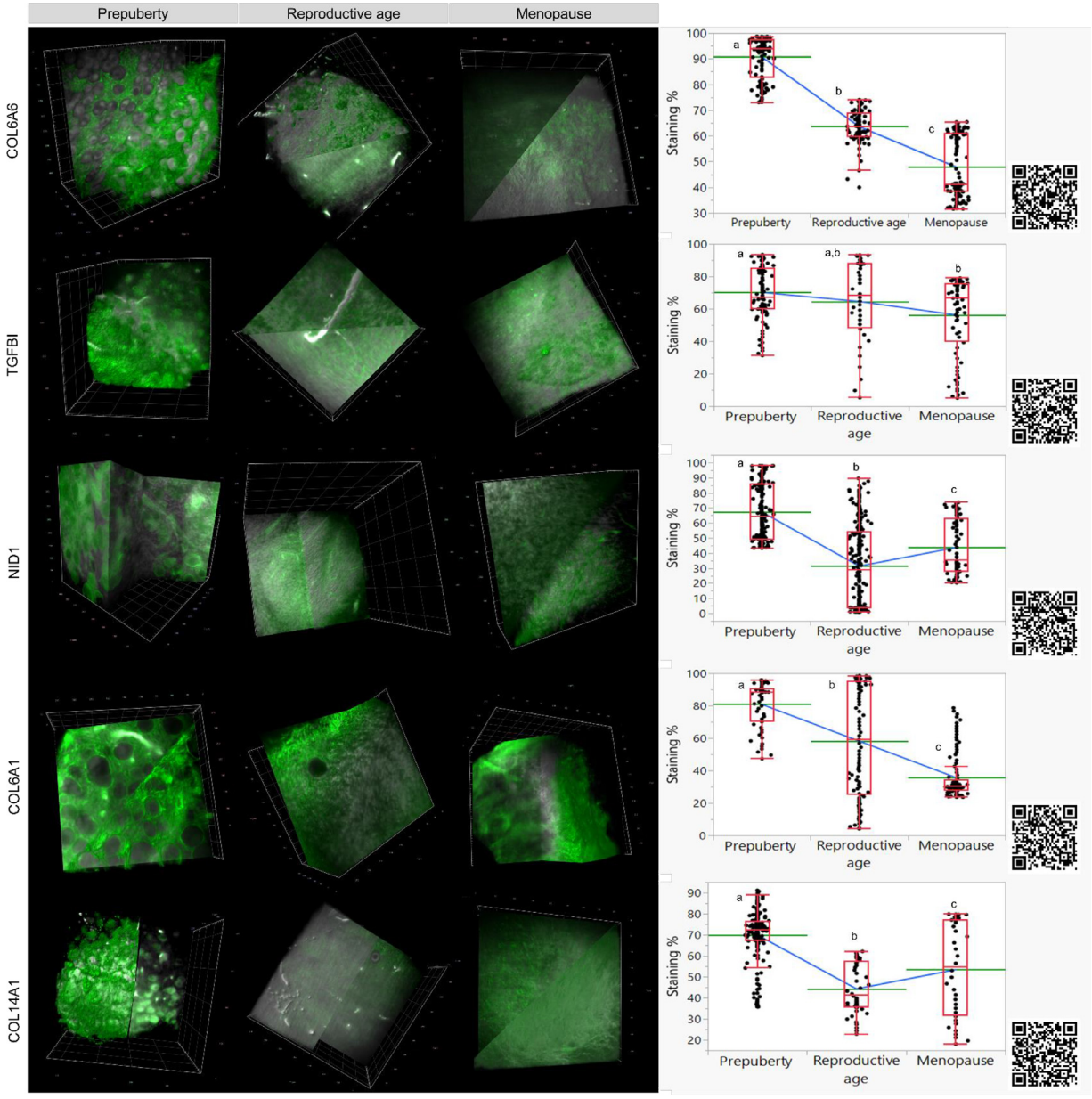

Fig. 5 Continued.

and IGF, and has been associated with development, morphogenesis, and cell proliferation [76]. It appears to be a very promising fertility biomarker, although its real implication in ovarian activity is still undercovered. Our neural network model further highlights the strong influence of GPC6 quantitative variations on the rest of ovarian matrisome protein expression. At the intracellular level, among the 45 upregulated proteins during reproductive age, many were implicated in nonsense mRNA decay (HNRNPL and TPI1), proper protein folding (P4HB, CALU, GPI, CALR, and TPI1), and senescence prevention (HNRNPD, ENO1, and FSCN1), highlighting the necessity of ubiquitous transcriptional as well as translational corrections to maintain normal ovarian function.

During reproductive life, the ovary undergoes continuous cyclic changes related to follicular development, requiring, therefore, continual angiogenesis [77], a process also promoted by AGT and GPC6. Nevertheless, upon menopause, the upregulation of COL18 corroborates with an important feature of aging, which is the marked reduction of the ovarian vascular network [78]. Indeed, a proteolytic fragment of COL18, endostatin, can downregulate VEGF-A and HIF-1α (upstream factor of VEGF-A), inhibiting

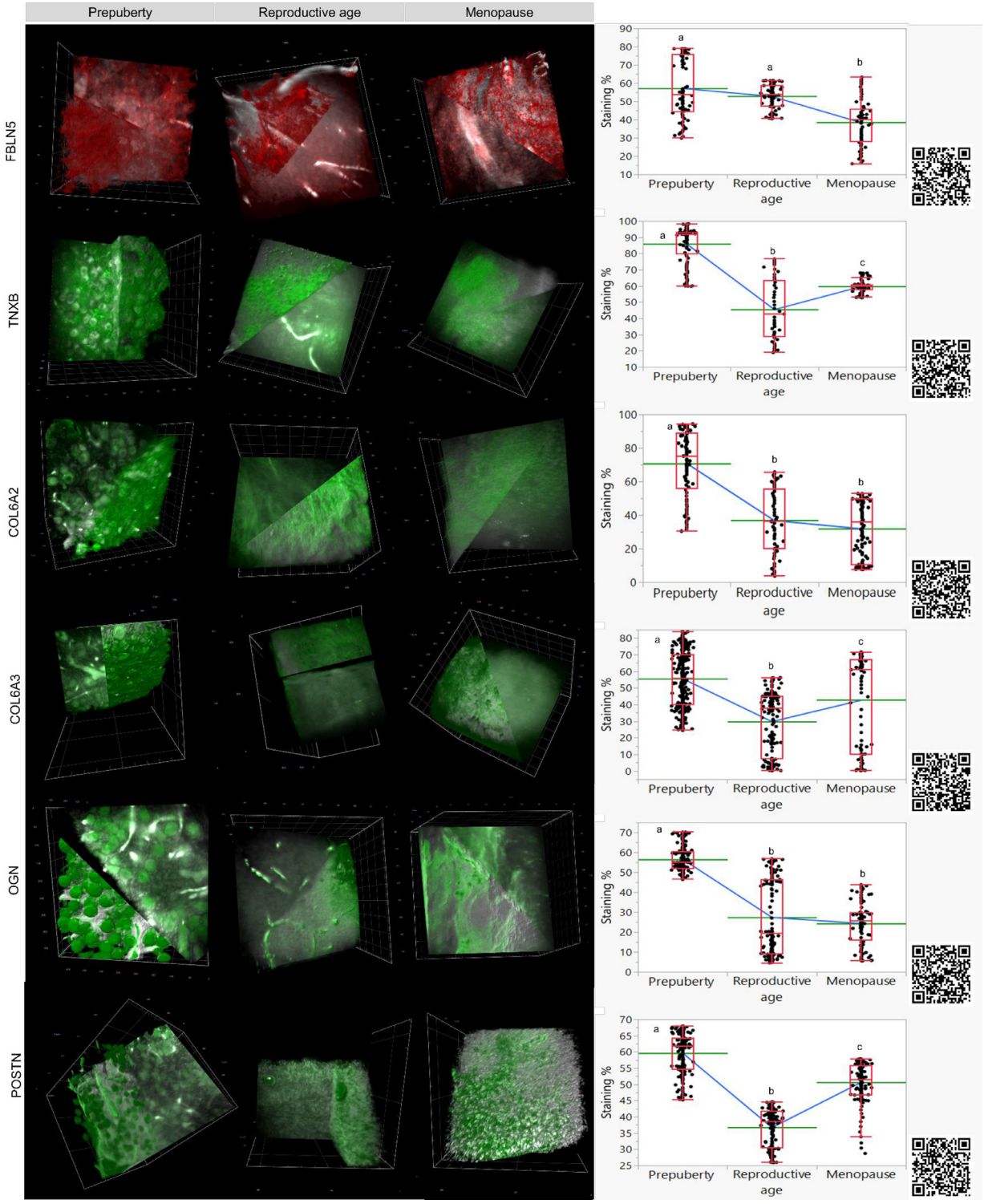

Fig. 5 Continued.

endothelial cell proliferation and negatively regulating angiogenesis [79].

On the other side, processes related to ECM remodeling and fibrosis were enriched with upregulated menopausal biomarkers at the matrisome level. Indeed, at this stage, the human ovary contains very few remaining follicles. Hence, follicular space has been consequently replaced by

neo-synthetized ECM, which sustains previous studies reporting age-related fibrosis (ANXA5, F2, ITIH4, and SERPINA1) in the human ovary [28]. Interestingly, the same matrisomal biomarkers of menopausal tissue implicated in fibrosis also play an essential protective role ranging from preventing ROS generation and cell damage to preventing heme toxicity (Fig. 6). Indeed, upregulated HPX during menopause plays a protectant role against hemoglobin (Hb)-derived heme toxicity resulting in ROS generation as well as mitigating heme-mediated effects on immune cells [80] that collectively contribute to driving inflammation [80] (Fig. 6). At the intracellular level, although markers of DNA fragmentation (PRF1 and IAPP), ROS generation (AOX1, PRF1, and CLIC1), and senescence (ARID4A, ZYX, and RBP1) were detected, proteins with cytoprotective roles, preventing DNA damage (PKM and PRDX6), oxidative-stress and ROS generation were also quantified (DDT, DBI, PSME1, and SLPI) (Fig. 7). ROS has been considered the most prominent molecular species involved in the aging process [81]. Indeed, all studies describing the aging process in different organs, including ovaries, have related aging to the downregulation of anti-oxidative stress pathways and/or ROS upregulation [82]. By contrast, our results reveal unique menopausal proteins with an anti-oxidative stress activity and highlight highly expressed proteins during adult life-fighting ROS generation inside-out the cells that increase with age (Figs. 6 and 7). Although cytoprotective anti-oxidative stress proteins detected in the menopausal group are more numerous than their antagonists and increase significantly with age, we are still unaware of their appropriate activity and function to counterbalance the ROS generation also detected during aging. Different scenarios may explain these results such as the lower turnover of these proteins and the implication of other ROS mechanisms, which prompts further investigations. Inflamm-aging is another hypothesis relating ovarian aging to inflammation [83]. In recent years, an increasing number of studies have found that inflammation is associated with the occurrence of aging, where tissues and organs are accompanied by a chronic, progressive proinflammatory state [84–86]. Interestingly, ovulation is an inflammation-like process during which the ovarian balance is achieved through proinflammatory action mediated by cytokines and negative feedback from anti-inflammatory cytokines, accompanied by leukocyte recruitment [47]. Hence, while it is not surprising to find proinflammatory proteins in reproductive age ovaries, some were equally expressed in menopausal ovaries (PSMB6, B2M) and others increased with age (CSRP1, IAPP, TSPO, PKM). In addition, detected high levels of AGEs at TBCK, SLITRK4 and HSPA8 activate intracellular multiple inflammatory signaling pathways [87], which corroborates the inflamm-aging hypothesis.

More surprising about the menopausal ovarian tissue is the upregulation of proteins related to cytokinesis and cell proliferation and even follicle activation. Thus, ovarian aging is not only associated with follicle senescence and prolonged dormancy of residual follicles, but it is also possibly related to inappropriate communication between menopausal ovarian cells and their microenvironment since follicles are hardly activated during menopause [88] despite the presence of several clues for their activation. This miscommunication can be attributed to collagen hypo-hydroxylation during menopause. Indeed, collagen hydroxylation promotes interactions with cellular collagen receptors, such as integrins and discoidin domain receptors, in both direct and indirect manners [31]. Moreover, proline hydroxylation may regulate the flexibility of collagen molecules and make functional sites available for interacting proteins [31]. Our previous findings also revealed that ovarian tissue aging is accompanied by tremendous architectural changes [50], limiting its porosity, which may hamper glucose, oxygen, and small molecule (cytokines, calcium) diffusion toward the ovarian cells. This would restrict the regulation of cellular processes that depend on these elements and bidirectional ECM-intracellular protein interactions.

At all stages of ovarian life, we have noted stimulatory and inhibitory proteins, mediating follicle activation or preventing it, namely at the level of mTOR and Hippo pathway to maintain homeostasis. Walter B. Cannon, the originator of the concept of homeostasis, said in his book Wisdom of the Body, ‘‘when a factor is known which can shift a homeostatic state in one direction it is reasonable to look for a factor or factors having an opposing effect’’[89]. But are these opposing factors at work all the time, or at least in some circumstances, might one factor prevail over the other and cause the rupture of homeostasis leading to pathology? Indeed, overexpression of AGT, SERPINA1, SERPINC1, POSTN, ANXA5, or F2 in PCOS compared to healthy patients is the best illustration of the importance of matrisome component harmonization at each age to comply with the ovarian physiological function at all stages of life (Fig. 8). This harmonization is described and effortlessly sensed by our data sonification technique orchestrating matrisome equilibrium and homeostatic remodeling from prepuberty until menopause. A disturbance of this equilibrium should change the generated expression melodies and alert of a potential pathological condition. Therefore, we forsee the potential of such a sonification technique in propelling MS use from the laboratory to the operating room by overcoming the difficulty of complex data processing and interpretation. This technique can be complementary to the emerging *in vivo*-MS and

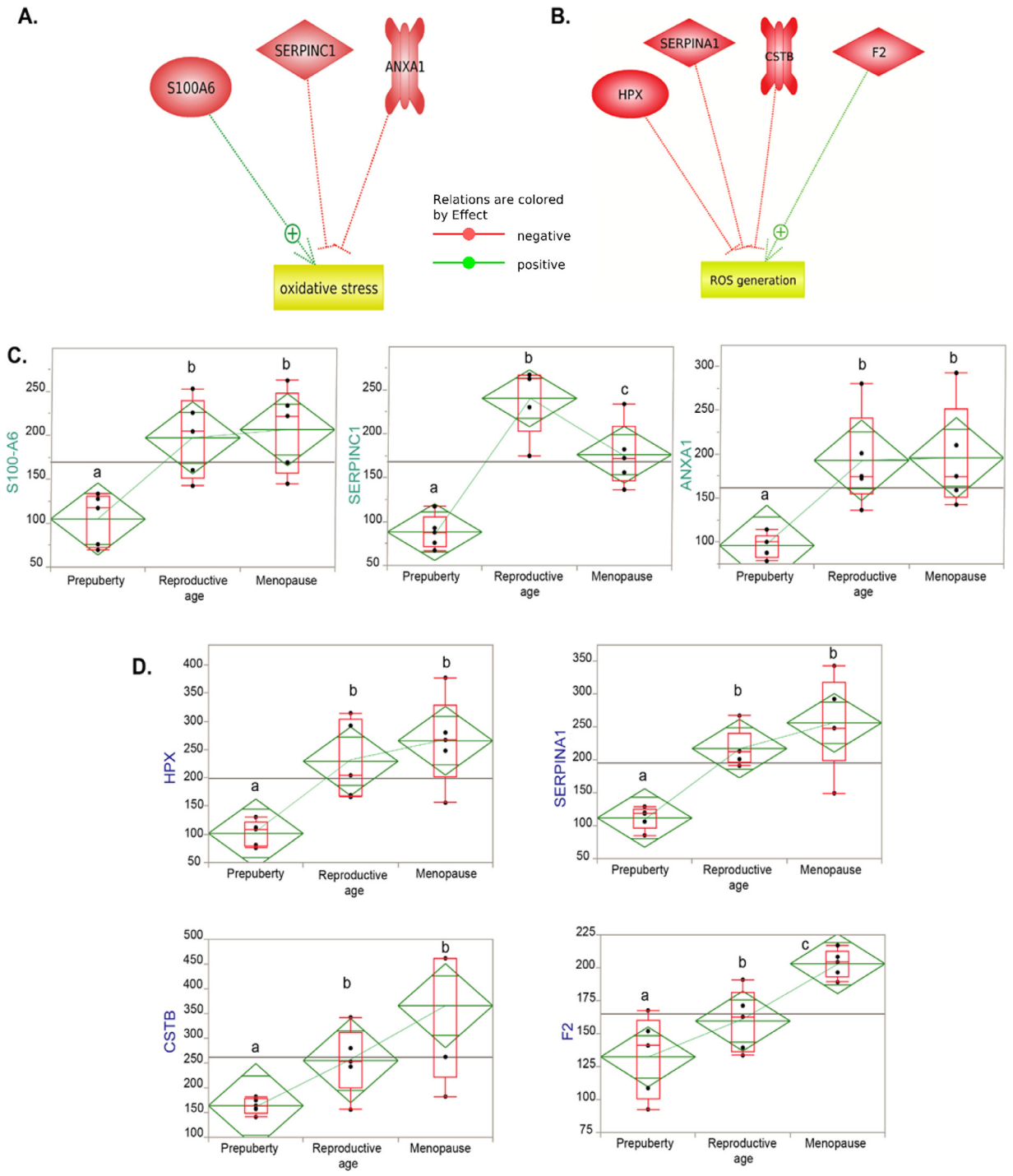

Fig. 6. ROS and oxidative-stress regulation under the control of matrisome proteins during ovarian life span.

A. Pro and anti-oxidative stress/ ROS regulators upregulated during adulthood (at reproductive- and menopausal age). B. An overall increase in the expression of matrisome proteins responsible of anti- ROS generation with age. References used by Pathway Studio to create relationships in A and B are reported in Supp Table 4. C-D. Box plots showing expression levels of selected proteins from prepuberty til menopause. Protein names are labeled according to their cluster highlighted in Fig. 2 (green is the cluster shared between reproductive-age and menopausal patients, the blue cluster refers to the proteins upregulated during menopause). Black dots indicate data points per patient. All box plots indicate median (center line), 25th and 75th percentiles (bounds of box), and minimum and maximum (whiskers). Means diamonds (95% confidence intervals for each mean) are also displayed. All paired comparisons were conducted with one way-ANOVA (post hoc: Tukey), different letters stand for statistical significance ($p<0.05$).

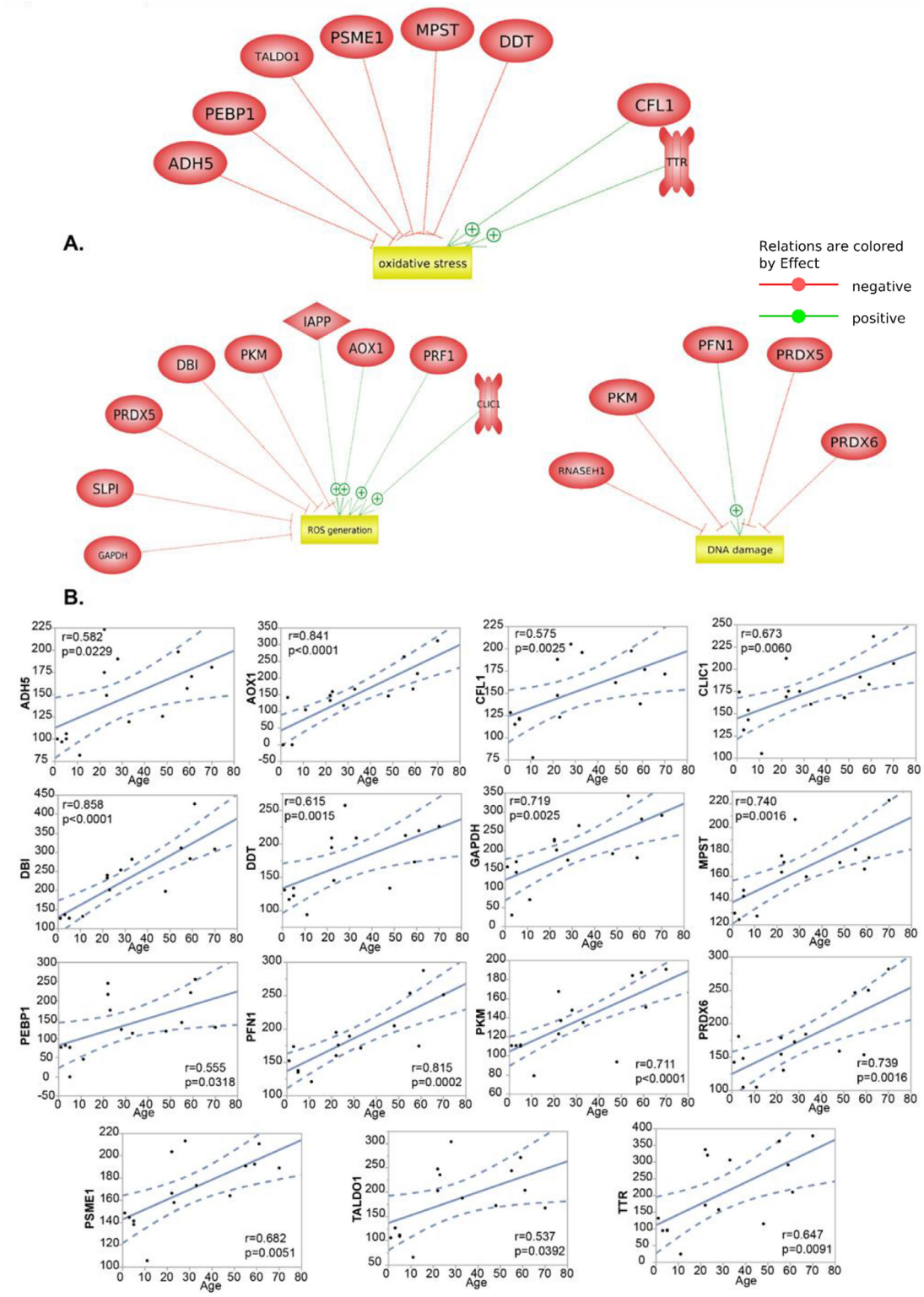

Fig. 7. Upregulated intracellular proteins during menopause regulating oxidative stress, DNA damage and ROS generation.

A. Graphical representation generated with pathway studio highlighting positive (green) and negative (red) regulation of oxidative stress, DNA damage and ROS generation under the control of intracellular proteins upregulated during menopause and highlighting the superiority in number of cytoprotective proteins. References used by Pathway Studio to create relationships in A are reported in Supp Table 4. B. Positive significant correlation (Pearson) between age and highlighted proteins in A.

Table 1. Used primary antibodies and respective parameters.Secondary antibodies recognizing mouse IgG (Invitrogen, #A21236) and rabbit IgG (Invitrogen, #A11034) were used at a 1/250 dilution. .

Antigen	Dilution	Company	Catalog number	Host
S100A6	1/50	Invitrogen	MA5−29,537	Mouse
SERPINC1	1/50	Proteintech	66,052−1-Ig	Mouse
HPX	1/100	Proteintech	66,479−1-Ig	Mouse
ITIH4	1/50	Proteintech	24,069−1-AP	Rabbit
SERPINA1	1/100	Proteintech	16,382−1-AP	Rabbit
COL6A6	1/50	Invitrogen	PA5−60,958	Rabbit
COL6A1	1/100	Proteintech	17,023−1-AP	Rabbit
AGT	1/50	Proteintech	11,992−1-AP	Rabbit
CLEC3B	1/50	Invitrogen	MA5−34,760	Rabbit
COL14A1	1/100	Invitrogen	PA5−104,514	Rabbit
CSTB	1/50	Proteintech	10,823−1-AP	Rabbit
COL18A1	1/50	Proteintech	18,301−1-AP	Rabbit
TGFBI	1/100	Proteintech	10,188−1-AP	Rabbit
ANXA7	1/200	Proteintech	10,154−2-AP	Rabbit
COL6A2	1/100	Proteintech	14,853−1-AP	Rabbit
ANXA1	1/100	Proteintech	66,344−1-Ig	Mouse
FBLN5	1/200	Proteintech	60,081−1-Ig	Mouse
HRNR	1/50	Invitrogen	PA5−56,756	Rabbit
OGN	1/50	Invitrogen	PA5−48,255	Rabbit
TNXB	1/50	Proteintech	13,595−1-AP	Rabbit
POSTN	1/50	Proteintech	19,899−1-AP	Rabbit
F2	1/50	Proteintech	24,295−1-AP	Rabbit
ANXA5	1/100	Proteintech	11,060−1-AP	Rabbit
NID1	1/50	Proteintech	13,766−1-AP	Rabbit
COL6A3	1/50	Invitrogen	PA5−49,914	Rabbit
GPC6	1/50	Invitrogen	PA5−53,622	Rabbit

may be used to pinpoint markers of cancer in a living patient's tissue during surgery, without having to wait for the pathology report that can take up to 45 risky minutes under anesthesia [90].

Due to its novelty, the current study may present certain limitations namely related to its descriptive aspect that relies on the prediction of the function of detected proteins in the ovary based on advanced literature text-mining, which will require further experimental validation.

The used proteomic workflow involves a collagenase mixture (LiberaseDH) digestion which might suggest the overcleavage of collagen type I and explain its underdetection comparerd to collagen VI. Nevertheless, the protein coverage of both collagen types were comparable which demonstrates the good identification of both collagen types with no preferential affinity of the collagenases and highlights the reliability of our results.

We believe that by dissecting the complexity of ovarian ECM in normal tissue throughout distinct developmental time points, our study provides important context for healthy ovarian physiology, identifying and characterizing disease states and recapitulating physiological tissues or development *in vitro*. To better understand the usefulness of ECM for regenerative medicine and tissue engineering applications, it is essential to have a more complete and comprehensive understanding of the ECM within normal, native tissue. Human ovarian matrisome until this day has remained incomplete and prevailed by knowledge built on animal models. Our data fill this gap and reveal potential biomarker candidates. Indeed, while highly expressed matrisome proteins at reproductive age can be promising candidates of fertility biomarkers at the ovarian tissue level, upregulated proteins during menopause could be considered potential ovarian aging biomarkers. This information may help the tremendous efforts that have been made to understand the increasing rate of female infertility, one of the top highest global disabilities of our era [91].

In this context, our findings pave the way for better-personalized oncology treatments and open new possibilities in oncofertility by providing a blueprint of the ovarian tissue toward creating new fertility restoration treatments for cancer patients such as functional bio-inspired engineered ovary mimicking the features of healthy reproductive-age tissue, the gold standard of fertility. Moreover, we provide an interactive model of ovarian matrisome that can predict the probability of a specific ovarian tissue matrisome to resemble prepubertal, reproductive-age, or menopausal tissue. This could be in the future a predictor of fertility potential, premature aging, or even an evaluation tool of the efficiency of ovarian rejuvenation or fertility restoration solutions acting at the level of the ECM. This model represents the first sparkle in computed gynecology and could become more robust by gradually introducing a higher number of analyzed healthy ovarian tissue.

At the intersection of fiber and cell theories, our study complements our knowledge of the human ovary during female life and opens new avenues in gynecology research and oncofertility practice (Supp Table 3). Our analytical method can be easily adapted to achieve a large-scale and in-depth quantitative analysis of ECM-containing proteome in other biological systems with relatively straightforward operations and low cost.

Funding

This study was supported by grants from the Fonds National de la Recherche Scientifique de Belgique (FNRS) (grant MIS #F4535 16 awarded to C. A. Amorim), Université Catholique de Louvain (PhD grant 'Coopération au développement' awarded and 'Mandats fin de thèse COVID' to E. Ouni) and CooperSurgical and Planer for sponsoring part of the experimental expenses.

CRediT authorship contribution statement

Emna Ouni: Methodology, Software, Formal analysis, Visualization, Investigation, Funding

Table 2. Matrisome biomarkers interaction with mTOR and Hippo pathways. To understand the possible interaction of ovarian matrisome biomarkers with key signalling pathways related to fertility and mainly follicle activation and development, we relied on pathway studio and its NLP technology (described in materials and methods) to study all the possible bidirectional regulation happening between each of the 26 matrisome biomarkers and members of Hippo or mTOR signaling pathways. All connections were manually supervised and curated to select the most relevant relationships between the matrisome and cellular proteins. Illustrations of all the described connections can be seen in supp Fig. 1 and supp Fig. 2 (---> Regulation; --+> Positif effect; ---| Negatif effect; ---- binding). An editable version of this table can be found on: https://data.mendeley.com/datasets/22t56fbd6t/draft?a=4b98519d-dfb4−4fe0-a1b0-b4e75b360be6.

Age group	Biomarkers	Biomarker-target relationship	Physiological impact	
Prepubertal	TGFBI	TGFBI ----> CDH1	Reduction in E-cadherin expression	Hippo pathway
		TGFBI ---+> CTNNB1	β-catenin stabilization and nuclear localization	
		SMAD1 ----| TGFBI	Impact on TGFBI expression and consequent arrest of cell proliferation	
	OGN	OGN ---+> CTNNB1	β-catenin stabilization and nuclear localization	
	POSTN	POSTN ----| TJP1	Impact on tight junction assembly and consequently on ovarian cell communication	
		POSTN ---+> TP73	E2F1 deNEDDylation / cell arrest and apoptosis activation	
		POSTN ----> CTNNB1	Regulation of Wnt/β-catenin signalling	
		TJP1 ----| POSTN	Downregulation of POSTN	
	COL6A3	COL6A3 ---+> YAP1	Stimulation of transcription activity, cell survival and growth	
	FBLN5	FBLN5 ----| ID1	DNA binding to transcriptional factors	
		FBLN5 ---+> WWTR1	TAZ activation via dephosphorylation and translocation to the nucleus	
		FBLN5 ---+> YAP1	Stimulation of transcription activity, cell survival and growth	
		FBLN5 ----| CTNNB1	Inhibition of Wnt/β-catenin signalling leading to potential follicle development	
Reproductive-age	GPC6	GPC6 ----| CTNNB1	Inhibition of Wnt/β-catenin signalling leading to potential follicle development	
	AGT	AGT ---+> CTNNB1	β-catenin stabilization and nuclear localization	
		CTNNB1 ---+> AGT	Activation of renin angiotensinogen system	
Reproductive-age & Menopausal	S100A6	S100A6 ----> CTNNB1	Possible implication in β-catenin degradation	
		S100A6 ---+> CDH1	Alteration of E-cadherin	
		YAP1 ---+> S100A6	Upregulation of S100A6	
		CTNNB1 ---+> S100A6	Upregulation of S100A6	
	ANXA1	ANXA1 ---+> CTNNB1	upregulation of Wnt/β-catenin signalling	
		ANXA1 ----| CDH1	negative regulation of E-cadherin	
		ANXA1 ---+> TJP1	Impact on tight junction assembly and consequently on ovarian cell communication	
		PARD3 ----- ANXA1	High levels of ANXA1 binding to PARD3 downregulate β-catenin expression	
Menopausal	F2	F2 ---+> PARD3	TAZ activation and cell growth by promoting LATS1 and PP1 interaction	
		F2 ----| TJP1	Impact on tight junction assembly and consequently on ovarian cell communication	
		F2 ---+> WWTR1	Tissue regeneration and wound healing	
		F2 ---+> LATS1	Activation of YAP/TAZ transcriptional activity	
		F2 ---+> 14_3_3	Stimulation of the association of 14-3-3 and RGS18 by increasing the phosphorylation of serine 49	
		F2 ---+> YAP1	Stimulation of transcription activity, cell survival and growth	
		F2 ----> CTNNB1	Adherens junction assembly	
	SERPINA1	SERPINA1 ---+> CDH1	Alteration of E-cadherin	
		SERPINA1 ---+> TJP1	Impact on tight junction assembly and consequently on ovarian cell communication	
		SERPINA1 ---+> PP2A	Stimulation of PP2 activity	
		TP73 ---+> SERPINA1	Upregulation of SERPINA1	
Prepubertal	COL14A1	COL14A1 ---+> SLC2A4	Glucose uptake	mTOR pathway
	OGN	OGN ---+> MAPK1	Enhancement of ERK1/2	
		OGN ----> INS	Glucose uptake	
		OGN ----| AKT1	downregulation of AKT activity	
		OGN ----| RHOA	Blocking cytoskeletal remodeling and cellular proliferation	
		AKT1 ---+> OGN	Upregulation of OGN	
		TP53 ---+> OGN	Upregulation of OGN by TP53 through a p53 specific binding region in OGN	
	COL6A1	COL6A1 ---+> AKT1	Akt activation	
		SREBF1 ----| COL6A1	Downregulation of COL6A1	
		glucose ---+> COL6A1	Upregulation of COL6A1	
	POSTN	POSTN ---+> STAT3	Upregulation of STAT3 and related stimulation of angiogenesis and proliferation	
		POSTN ---+> BCL2L1	Inhibition of cell death through upregulation of BCL2L1	
		POSTN ----| PPARG	Suppression of PPARG expression and modification of related lipid metabolism	
		POSTN ---+> TP53	Stabilization of p53 and positive regulation of apoptosis	
		POSTN ---+> MAPK1	Increased phosphorylation of ERK and Akt	
		POSTN ---+> RPS6KB1	Stimulation of RPS6KB1 activation	
		POSTN ---+> INS	Increase insulin activity	
		POSTN ---+> MTOR	Stimulation of mTOR signalling through binding to integrin and activation of integrin-linked kinase (ILK)	
		POSTN ---+> PI3K	Activation of PI3K via integrin binding and focal adhesion kinase activation	
		POSTN ---+> AKT1	Increased phosphorylation of Akt and mTOR downstream targets	
		POSTN ---+> RHOA	Increased activation of RHOA by thyrosine phosphorylation of focal adhesion-> stymulation of actin polymer	
		POSTN ----| GSK3B	Inhibition of BSK3B, a major regulator of Wnt/β-catenin signalling	
		POSTN ----| PTEN	blockage of PTEN and consequent decrease in β-catenin degradation	
		RPS6KB1 ---+> POSTN	Activation of periostin-induced actin polymerization	
		glucose ---+> POSTN	Induction of POSTN expression under high glucose concenration	
		PI3K ---+> POSTN	Mediation of periostin expression	
		Ras GTPase ----> POSTN	Induction of POSTN expression through Angiotensin II	
		MAPK1 ---+> POSTN	Induction of POSTN expression through MAPK/ERK	
		STAT3 ----> POSTN	Regulation of POSTN expression through binding to its promoter	
		YY1 ----| POSTN	Negative modulation of POSTN transcription	
		PPARG ----| POSTN	Downregulation of POSTN	
	HRNR	HRNR ---+> AKT1	Akt phosphorylation	
	TGFBI	TGFBI ----> MTOR	mTOR activity regulation	
		TGFBI ---+> TP53	Upregulation of p53 expression and regulation of DNA repair	
		TGFBI ----| GSK3B	Inhibition by phosphorylation and activation of canonical Wnt pathway and consequent β-catenin stabilizatio	
		TGFBI ---+> PXN	Phosphorylation of PXN	
		TGFBI ---+> AKT1S1	Upregulation of AKT1S1	
		TGFBI ---+> PXN	Activation of FAK-paxillin signaling and cytoskeleton reorganization	
		TGFBI ---+> EIF4EBP1	Upregulation of EIF4EBP1 and downstream mTOR activity regulation	
		TGFBI ---+> RPS6	Upregulation of RPS6 and regulation of protein synthesis	
		TGFBI ---+> F-actin	Densification of F-actin	
		TGFBI ---+> AKT1	Phosphorylation and activation of Akt	
		IGF1 ---+> TGFBI	Upregulation of TGFBI	
		glucose ---+> TGFBI	Upregulation of TGFBI	
	FBLN5	FBLN5 ---+> AKT1	FBLN5 expression requires pi3k/Akt/mTOR activation	
		FBLN5 ---+> MAPK1	Stimulation of TGF-β-induced activation of MAPK	
		FBLN5 ---+> GSK3B	Activation of GSK3B, which degrades β-catenin	
		PPARG ---+> FBLN5	Increased expression of FBLN5	
		IRS2 ----| FBLN5	Downregulation of FBLN5	
		glucose ----> FBLN5	Regulation of FBLN5 expression via glucokinase-mediated gluose signaling	
		MTOR ---+> FBLN5	Increase in FBLN5 transcriptional level	
		PI3K ---+> FBLN5	Stimulation of hypoxia-induced FBLN5 expression	
	COL6A3	COL6A3 ----| PPARG	Downregulation of PPARG and related lipid metabolism	
		PPARG ----| COL6A3	Suppression of COL6A3 expression	
		IRS1 ---+> COL6A3	Upregulation of COL6A3	
	ANXA7	ANXA7 ----| PRKCA	Downregulation of PRKCA	
		ANXA7 ---+> STAT3	Upregulation of STAT3	
		ANXA7 ---+> ATG13	Upregulation of ATG13 and increased autophagy	
		GSK3B ---+> ANXA7	Upregulation of ANXA7	
		TP53 ----> ANXA7	ANXA7 is indirect substrate of p53	
		PKA ----> ANXA7	ANXA7 phosphorylation	
Reproductive-age	AGT	AGT ---+> MTOR	mTOR positive regulation	
		AGT ---+> SREBF1	mTOR activation	
		Ras GTPase ----| AGT	Reduction of systematic RAS activity	
		PPARG ----| AGT	Downregulation of Wnt/β-catenin signalling	
		IGF1 ---+> AGT	Upregulation of AGT	
		INS ---+> AGT		
		IGF1 ---+> AGT		
		glucose ---+> AGT		
		RHOA ----> AGT	Stressed-induced activation of Rhoa dfferently regulate AGT	
		MAPK1 ---+> AGT	Upregulation of AGT	
		PKA ---+> AGT	Upregulation of AGT	
		PRKCA ----| AGT	Inihibition of AGT expression	
		KRAS ---+> AGT	Activation of AGT experssion	

Reproductive-age & Menopausal	SERPINC1	SERPINC1 ---+> IGF1	Enhancement of IGF1 production	mTOR pathway	
		SERPINC1 ----> glucose	Glucose oxydation		
		SERPINC1 ----> PI3K	Regulation of mTOR/PI3k/Akt activation		
		SERPINC1 ----> AKT1			
		SERPINC1 ----> MAPK1	Inhibition of the phosphorylation of ERK 1/2, p38 MAPK and dowstream cytokines		
		SERPINC1 ---+> PKA	Activation of PKA		
		SERPINC1 ----> ULK1	AMP-activated protein kinase downstream phosphorylation of ULK1, a known modulator of autophagy		
		SERPINC1 ---+> AMPK	Upregulation of AMPK signaling		
		SERPINC1 ----> MTOR	Increased phosphorylation of Mtor, Pi3k and Akt		
		TP53 ----| SERPINC1	Downregulation of SERPINC1		
		INS ---+> SERPINC1	Stimulation of SERPINC1		
		glucose ----| SERPINC1	Dose-dependant decrease of thrombin secretion		
	ANXA1	ANXA1 ---+> F-actin	ANXA1 binds to and bundle actin filament		
		ANXA1 ---+> PPARG	Upregulation of PPARG by phosphorylation of STAT6		
		ANXA1 ---+> PXN	Stimulation of PXN phosphorylation		
		ANXA1 ---+> MAPK1	Mediation of ERK activation		
		ANXA1 ---+> RHOA	Increased RHOA activation		
		ANXA1 ----> EIF4E	Modification of lipopolysaccharide-induced phosphorylation of EIF4E		
		ANXA1 ----> AMPK	AMPK activation		
		ANXA1 ----> AKT1	Akt phosphorylation		
		ANXA1 ---+> TP53	Upregulation of p53 transcritional ativity and related pro-apoptic signalling		
		ANXA1 ----| INSR	Dose-dependant inhibition of INSR auto-phosphorylation		
		ANXA1 ---+> STAT3	Increased phoshorylation of STAT3		
		ANXA1 ---+> RHOA	F-actin stabilization via binding to G-actin		
		ANXA1 ----> MTOR	context-dependant regulation of mTOR signalization		
		ANXA1 ----| PI3K	Downregulation of AKT phosphorylation		
		ATP ---+> ANXA1	ANXA1 secretion under ATP hydrolysis		
		ANXA1 ----> 14_3_3	Anti-inflammatory effect by binding		
		INSR ----> ANXA1	ANXA1 Substrate for phosphorylation by INSR		
		PKA ---+> ANXA1	ANXA1-PKA dependant expression		
		AKT1 ---+> ANXA1	Upregulation of ANXA1		
		glucose ---+> ANXA1	Increased transcriptional level of ANXA1		
		GSK3B ----| ANXA1	Downregulation of ANXA1		
		phosphatidic acid ---+> ANXA1	ANXA1 translocation to plasma membrane		
		PI3K ---+> ANXA1	Phosphorylation and translocation of ANXA1		
		PPARG ---+> ANXA1	Induction of ANXA1 expression		
		PP2A ----> ANXA1	ANXA1 phosphorylation dependant on PKCA-PP2A activity		
		PRKCA ----> ANXA1			
	S100A6	S100A6 ---+> MAPK1	Phosphorylation and upregulation of MAPK1		
		S100A6 ----> MAPT	Regulation of TAU/ MAPT through activation of PPP5C (dephosphorylation role)		
		S100A6 ---+> TP53	Activation of p53		
		S100A6 ---+> AKT1	Positive regulation of Akt signaling		
		S100A6 ----> STAT3	Upregulated phosphorylation of STAT3		
		STAT3 ---+> S100A6	Upregulation of S100A6 by YAP-phosphorylated STAT3		
		PI3K ---+> S100A6	Upregulation of S100A6 expression		
		TP53 ----| S100A6	Suppression of S100A6 promoter		
		MAPK1 ---+> S100A6	Upregulation of S100A6		
	HPX	HPX ---+> AKT1	Akt activation through MMP-9 domain of HPX		
		HPX ---+> TP53	Upregulation of p53 by heme-HPX		
		HPX ---+> RHOA	Alteration of cytoskeletal distribution		
		HPX ---+> F-actin	Reorganization of filamentous actin via MMP-3 domain of HPX		
		HPX ---+> MAPK1	MAPK activation by HPX- MMP-9 domain binding to integrin and CD44		
		INS ----| HPX	Downregulation of HPX		
		glucose ---+> HPX	Upregulation of HPX under glucose induced-oxidative stress		
		ATP ----| HPX	Inactivation of HPX by forming a complex with ATP		
	ANXA5	ANXA5 ---+> TP53	Upregulation of p53 possibly via Fas pathway		
		ANXA5 ----- F-actin	ANXA5 binding to actin		
		ANXA5 ----| PRKCA	Inhibition of PRKCA activity		
		ANXA5 ----| Ras GTPase	Suppression of RAS activation by decreasing the association of Shc with Grb2		
		ANXA5 ----| GRB2			
		TP53 ---+> ANXA5	Upregulation of ANXA5 by binding to its promoter		
		MAPK1 ---+> ANXA5	Induced expression of ANXA5 via ERK1/2 signalling		
		TERT ----| ANXA5	Inhibition of ANXA5 and promotion of cell growth		
		INS ---+> ANXA5	High glucose uptake stimulates ANXA5 expression		
		glucose ---+> ANXA5			
		IGF1 ---+> ANXA5	Increased ANXA5 binding		
		PTEN ---+> ANXA5	Upregulation of ANXA5		
		PKA ----> ANXA5	PKA-dependant phosphorylation between follicular and luteal phase		
		PRKCA ---+> ANXA5	Upregulation of ANXA5		
	COL18A1	COL18A1 ----| TP53	Downregulation of p53		
		COL18A1 ----| RAF1	Inhibition of RAF1 phosphorylation and its downtream MEK1/2 target		
		PTEN ---+> COL18A1	Upregulation of COL18A1		
		TP53 ---+> COL18A1	Activation of the COL18A1 encoding		
		YY1 ----> COL18A1	Interaction with COL18A1 gene promoter and regulation of its expression		
Menopausal	F2	F2 ---+> PIP3	Stimulation of PIP3 formation	mTOR pathway	
		F2 ---+> phosphatidic aci	Phasphatidic-acid thrombin production		
		F2 ---+> glucose	Stimulation of glucose metabolism		
		F2 ---+> SGK1	Induction of SGK1 expression		
		F2 ---+> SLC2A4	Uprergulation of SLC2A4		
		F2 ----> MAPK1	Stimulation of ERK1/2 activity		
		F2 ----| IGF1	Downregulation of IGF1 in a dose related manner		
		F2 ---+> TP53	Induction of p53 expression		
		F2 ---+> IGF1R	Upregulation of IGF1R		
		F2 ----> RHOA	RHOA translocation		
		F2 ----> GRB2	Tyrosine phosphorylation of GRB2		
		F2 ---+> PRKCA	Activation of PRKCA		
		F2 ---+> IRS1	Induced ROK-α/IRS-1 association		
		F2 ---+> SHC1	Upregulation of SHC1 phosphorylation		
		F2 ---+> AKT1	Phosphorylation and activity maintenance of Akt by thrombin		
		F2 ----> PKA	context-dependant regulation of PKA		
		F2 ---+> MAPT	Hyperphosphorylation and MAPT aggregation		
		F2 ---+> PDPK1	Stimulation of PI3K/Akt signalling		
		F2 ---+> Ras GTPase	Ras activation		
		F2 ----> calmodulin	Stabilization of calmodulin		
		F2 ---+> AMPK	AMPK activation		
		F2 ---+> PXN	Increased PXN phosphorylation		
		F2 ---+> TORC2	stimulatIon of Akt phosphorylation at serine 473, an important mTOR complex 2 target		
		F2 ---+> PI3K	Activation of PI3K/Akt		
		F2 ---+> RPS6KA1	Activation of RPS6KA1		
		F2 ---+> MTOR	Activation of Mtor signaling		
		F2 ---+> 14_3_3	Increased 14-3-3 binding		
		F2 ----> FOXO3	Phosphorylation of FOXO3		
		F2 ----> IQGAP1	Assembly of IQGAP1		
		F2 ---+> RPS6KB1	Stimulation of RPS6KB1 activity		
		F2 ---+> F-actin	Stimulation of F-actin bundling		
		F2 ---+> RAF1	RAF1 phosphorylation		
		F2 ---+> GSK3B	Dephosphorylation and activation of GSK3		
		F2 ---+> SREBF1	Increase in precursor and active forms of SREBF1		
		F2 ---+> STAT3	Phosphorylation of STAT3		
		INS ---+> F2	Potentitation of thrombin mitogenic activity		
		glucose ---+> F2	Increased thrombin activation		

acquisition, Writing – original draft. **Valerie Nedbal:** Formal analysis. **Marta Da Pian:** . **Hangbao Cao:** . **Kalina T. Haas:** . **Alexis Peaucelle:** . **Olivier Van Kerk:** Investigation. **Gaetan Herinckx:** . **Etienne Marbaix:** . **Marie-Madeleine Dolmans:** . **Timo Tuuri:** . **Marjut Otala:** . **Christiani A. Amorim:** Methodology, Resources, Funding acquisition, Writing – review & editing. **Didier Vertommen:** Methodology, Investigation, Writing – review & editing.

Declaration of competing interests

All authors have no competing interests to declare

Acknowledgments

We thank the SMCS platform (Louvain Institute of Data Analysis and Modeling in Economics and Statistics, Université Catholique de Louvain) for their guidance and advice on the used statistical tests. We highly appreciate the Kidney and Pancreatic Transplantation Unit of UCLouvain's Saint-Luc Hospital for the donation of ovaries and the help of Valentina Alabani and Elsa Seijnhaeve from the pathology department of Saint-Luc Hospital in collecting the fixed ovarian samples used in immunofluorescence. We are also thankful to Paolo Chiappa for his technical assistance with JMP Genomics software and Samy Memmi and Sergei Snovida from Thermo Fischer for their help with the experimental design using 16-plex TMT pro. We thank Proteintech for generously providing free antibody samples that have been used in immunofluorescence. We are grateful to Mira Hryniuk for reviewing the English language of the manuscript.

Supplementary materials

Supplementary material associated with this article can be found in the online version at doi:10.1016/j.matbio.2022.03.005.

Experimental Procedures

Ovarian biopsies included in this study

The use of the human ovarian cortex was approved by the Institutional Review Board of the Université Catholique de Louvain on May 13, 2019 and May 25, 2019 (IRB references 2012/23MAR/125 and 2018/19DEC/475). Ovarian tissue from prepubertal girls was donated by patients treated at the Children's Hospital and the Department of Obstetrics and Gynecology of the University Central Hospital of Helsinki (Finland). Pediatric patients from Children's Hospital in Helsinki participated in a fertility preservation program and a research project approved by the Ethics Committee of Helsinki University Central Hospital (license number 340/13/03/03/2015). Written informed consents for pediatric patients were given by their guardians and by all age-appropriate patients.

Ovarian cortex biopsies were taken from prepubertal (mean age [±SD]=7±3 years; n=5), reproductive-age (mean age [±SD]=26±5 years; n=5) and menopausal (mean age [±SD]=59±8 years; n=5) patients after obtaining their informed consent. All participating adult subjects were undergoing laparoscopic surgery for benign gynecological diseases not affecting the ovaries. All samples used in mass spectrometry analyses were cryopreserved by slow freezing [92] and kept frozen until the day of their analysis. Samples used in imagery analyses were obtained from the pathology department of Université Catholique de Louvain St-Luc's Hospital after overnight fixation in 4% paraformaldehyde. They were kept in 70% ethanol until the day of their processing, as described below.

Protein extraction

All samples were processed throughout the entire procedure simultaneously on the same day to avoid batch effects. First, cryopreserved samples were thawed [92] and cut into 3 x 3 x 1 mm fragments using graph paper. The excess medium was removed with gauze, and the 10 mg wet weight of each sample was processed following our DC-MaP technique [10]. Briefly, each 10 mg-ovarian tissue was transferred to an empty 2 mL FastPrep®Lysing matrix tube (MP Biomedicals) filled with 200 µL lysis buffer (0.2% RapiGest [Waters Corp., Milford, MA], 300 mM NaCl 25 mM HEPES, 0.25 mM sodium orthovanadate, 50 mM NaF, 0.25 mM PMSF, 1X halt protease inhibitor cocktail [Thermo Scientific, San José, USA] and 5 mM EDTA) and mechanically lysed using 0.3 mm-diameter stainless steel beads (Full Moon, BioSystems, Sunnyvale, CA, USA). Homogenization was carried at 4°C with Precellys Evolution (Bertin Technologies, Montigny-le-Bretonneux, France). The homogenate was eluted with the needle technique [10] by centrifugation at 3000 g for 5 min at 4°C. The eluate was then centrifuged again at 16,000 g for 30 min at 4°C to recover the supernatant, representing the soluble fraction.

The remaining pellet representing the insoluble fraction was enzymatically digested using 1.35 mg/mL LiberaseTM DH (Roche Diagnostics, GmbH, Mannheim, Germany) in 100 mM triethylammonium bicarbonate (TEAB, pH 8) and 5 mM CaCl2. Each sample was subsequently incubated at 37°C for 2 h under agitation (140 rpm) with regular 30-s vortexing

every 30 min. The enzymatic reaction was halted by the addition of 20 mM EDTA. Both soluble and insoluble fractions were processed as described below.

Soluble fraction processing

One hundred μg of total soluble proteins were reduced with 5 mM 1,4-Dithiothreitol (DTT), incubated for 30 min at 56 °C, and subsequently alkylated with a 25 mM final concentration of chloroacetamide for 25 min at room temperature in the dark. The proteins were then precipitated using methanol-chloroform, resuspended in 100 mM TEAB (pH 8), and further digested with Lys-C/trypsin at an enzyme:substrate ratio of 1:25 [wt/wt] overnight at 37 °C. The samples were centrifuged at 16,000 g for 10 min at 4 °C. Recovered peptides were quantified by Pierce™ Quantitative Colorimetric Peptide Assay (#23,275, Thermo Scientific) according to the manufacturer's instructions.

Insoluble fraction processing

One hundred μg of total insoluble proteins were resuspended in a 6 M final concentration of urea in 100 mM TEAB, with continuous vortexing and sonication. Proteins were then reduced in 5 mM DTT and incubated for 1 h at 37 °C. After cooling to RT, cysteines were alkylated by adding 25 mM chloroacetamide for 25 min at RT in the dark. No precipitation was conducted during insoluble fraction processing to avoid resolubilization problems and take advantage of the trypsin-enhancing action of RapiGest. Protein digestion was performed using Lys-C/trypsin at an enzyme:substrate ratio of 1:50 [wt/wt] and incubation for 2 h at 37°C under 1000 rpm agitation. After reducing urea concentration to 1 M by adding 100 mM TEAB, a second aliquot of trypsin was added to the sample at an enzyme:substrate ratio of 1:100 [wt/wt] and incubated overnight at 37°C with continuous agitation at 1000 rpm. The reaction was stopped and the detergents hydrolyzed by the addition of freshly prepared 50% trifluoroacetic acid (TFA) [vol/vol] to a final concentration of 1% TFA [vol/vol], pH < 2. The acidified sample was centrifuged at 16,000$\times$ g for 10 min at RT to eliminate the insoluble MS-compatible detergents. Digests were then desalted and concentrated on HyperSep C18 cartridges (50 mg/mL, Thermo Scientific, San Jose, CA, USA) according to the manufacturer's instructions and then dried using a speedvac. Peptides were resuspended in 50 μL of 100 mM TEAB and quantified by the Pierce™ Quantitative Colorimetric Peptide Assay following the manufacturer's instructions.

TMTpro labelling

Thirty μg of peptides were prepared in one hundred μl of 100 mM TEAB. In addition, a bridge sample, which contains an equal amount (1 μg) of each soluble and insoluble fraction, for a total of thirty μg, was prepared in one hundred μl of 100 mM TEAB. All were labeled with TMTpro™ 16-plex Label (A44521, Thermo Scientific) according to the manufacturer's instructions (Fig. 1). One label reagent (reporter ion) was used for the bridge sample, and the fifteen other labels were used to label an equal amount of peptides from the soluble and insoluble fractions. After labeling with the TMT tags and quenching the reaction with 5 μL of 5% hydroxylamine, an equal amount of each soluble fraction and bridge sample were combined on one side. And the same equal amount of each insoluble fraction and the bridge were mixed on the other side. Both combined samples were dried in a speedvac, resuspended in 3.5% acetonitrile (ACN) [vol/vol] and 0.1% TFA [vol/vol] in water, then cleaned up with C18 cartridges (200 mg/mL, Thermo Scientific) according to the manufacturer's instructions then dried again and resuspended in 3.5% ACN [vol/vol] and 0.1% TFA [vol/vol] in water.

Liquid chromatography-tandem-mass-spectrometry (LC-MS/MS)

One μg of peptides dissolved in solvent A (0.1% TFA in 2% ACN) was directly loaded onto a reversed-phase pre-column (Acclaim PepMap 100, Thermo Scientific) and eluted in backflush mode. Peptide separation was achieved using a reversed-phase analytical column (Acclaim PepMap RSLC, 0.075 $\times$ 250 mm, Thermo Scientific) with a 140 min linear gradient of 4%−32% solvent B (0.1% TFA in 80% ACN) for 99 min, 32%−60% solvent B for 10 min, 60%−95% for 1 min and holding at 95% for the last 10 min at a constant flow rate of 300 nL/min on an Ultimate 3000 RSLN nanoHPLC system (Thermo Scientific). The peptides were analyzed by an Orbitrap Fusion Lumos tribrid mass spectrometer (Thermo Fisher Scientific) with enabled advanced peak determination (APD) and relative quantification either by MS2 or SPS MS3. The peptides were subjected to a nanospray ionization source, followed by MS/MS in the Fusion Lumos coupled online to the UPLC. Intact peptides were detected in the Orbitrap at a resolution of 120,000 with a scan range m/z from 375 to 1500 and an AGC target of $4x10^5$, maximum injection time was set to 50 ms. A data-dependent procedure of MS/MS scans was applied for the top precursor ions above a threshold ion count of 5.0×10^3 in the MS survey scan with 60 s dynamic exclusion. The total cycle time was set to 3 s. For MS2 quantification of the TMT reporter ions, MS/MS spectra were acquired in the Orbitrap at a resolution

of 50,000 after HCD fragmentation at 35% with an AGC target of 1×10^5 ions and a maximum injection time of 120 ms. For MS3 quantification, MS/MS spectra were first acquired in the Ion Trap after CID fragmentation at 30%, 10 precursors were synchronously selected (SPS MS3) for HCD fragmentation at 55%, and the MS3 spectra was acquired in the Orbitrap at a resolution of 50,000 with an AGC of 2 x 10^5 and a maximum injection time of 120 ms. MS/MS spectra was exported using the following settings: peptide mass range: 350−5000 Da, minimal total ion intensity: 500.

Protein identification and quantification

The resulting MS/MS data were processed using the Sequest HT search engine within Proteome Discoverer 2.4 against a human protein reference target-decoy database obtained from Uniprot (March 1, 2020, 87,489 forward entries). Trypsin was specified as the cleavage enzyme, allowing up to 2 missed cleavages, 4 modifications per peptide, and up to 3 charges. The mass error was set to 10 ppm for precursor ions and 0.1 Da for fragment ions and considered dynamic modifications were +15.99 Da for oxidized methionine or proline, +21.984 Da for glyoxal on arginine, +114.042 Da for 3-deoxyglucosone on arginine, and +42.011 Da for acetylation of the protein N-term. Fixed modifications were TMTpro (+304.207 Da) for lysine and peptide N-termini and +57.00 Da for carbamidomethyl cysteine. The false discovery rate (FDR) was calculated using Percolator, and thresholds for protein, peptide, and modification sites were specified at 1%. Relative quantification was performed with the MS2 or MS3 signal from TMT reporters' ions. Quan value corrections for isotopic impurities were applied, and the co-isolation threshold was set at 50 or 65 for MS2 and MS3 data respectively. Two different ways of normalization were used: none with a scaling mode set on "controls average" or "all average"; or with normalization against a specific protein database containing Liberase.

Proteomic data post-processsing and statistical analysis

Only proteins that have been identified with at least 2 unique peptides per protein have been taken into consideration. Since our DC-Map technique leads to the obtention of two fractions, soluble and insoluble, to have an optimal quantification of the total amount of a protein per ovarian tissue, we summed its intensity in both fractions. Missing intensities from MS2 were replaced by MS3 for all compared samples. Matrisome protein recognition in Sequest result files was achieved by comparison of confidently detected proteins with the Matrisome Project data set (http://matrisomeproject.mit.edu/), an in silico-identified ECM protein set founded on the characteristic domain-based organization of ECM proteins. Quantile normalization has been used to normalize cellular and extracellular data distribution. Bioinformatics analyses, including Pearson's correlation analysis, hierarchical clustering, parallel plots, and volcano plots have been conducted on JMP Genomics 10. For biomarker discovery, a one-way ANOVA analysis with an FDR cutoff of 0.05 was used and carried on JMP Genomics 10. Biological processes and pathways were enriched with Pathway Studio using GSEA. At least two selected terms with $p<0.05$ were shown for each cellular process.

Data-mining

Pathway Studio (www.pathwaystudio.com) was used to examine possible interactions of matrisome proteins of interest with other cellular proteins and explore the biological processes they are involved in. Pathway Studio is an Elsevier-associated text-mining software that collects more than 13.5 million biological relationships between different entity types, including genes, diseases, drugs, and cells. It gets updated weekly and covers over 32 million PubMed abstracts and 5.3+ Elsevier and third-party full-text articles. The database was compiled using an NLP technology called MedScan [93].

Machine learning (neural network)

Using the 26 matrisome biomarkers differently, distinguishing each age group, we constructed a neural network via JMP genomics by building a model predicting the interdependence of matrisome protein intensities. The constructed model also calculates the probability of an ovarian tissue matrisome analyzed with our described pipeline to resemble prepubertal, reproductive-age, or menopausal tissue. Through its interactive interface, the model demonstrates how by shifting the expression level of one or several matrisome proteins, the biological tissue age might be changed. To do so, the dataset was split into training (60% of total data), validation (20%), and testing (20%) following the Holdback validation method to ensure the model performance.

Data sonification

Sonification translates data into a sound signal that helps integrate multi-parameter data. The following parameters could be used simultaneously to generate a soundtrack: pitch level, intensity, and rhythm.

To illustrate the evolution of relative protein representation in the tissue, we focused on pitch to represent the level of protein expression: the higher the

pitch, the higher the relative expression. We will not use the intensity as a marker as our ear interpret pitch and intensity in a nonlinear relation. Thus, this parameter could lead to misinterpretation of the data. Played one by one, we could follow the melody of 3 soundtracks describing the evolution of matrisome composition from prepubertal toward menopausal age that we name "expression melodies." We could then play together several "expression melodies" combining similar matrisome categories (eg., proteoglycans, collagens) corresponding to each age. The diversity in pitch or the richness of the obtained choir will represent the diversity in expression levels within this category. The evolution will pinpoint global changes affecting part or all the quantified matrisome components. To facilitate the audition, we used a rhythm-based on three beats (3-time points) to express the transition from one type of category to the other at each step. This way, we can hear the orchestration of the biochemical evolution of ECM during aging.

The data was sonified as follows. First, we took an average (AV) and standard error of the mean (SEM) over all the repetitions for each age group and a given category (e.g. collagens). The amplitude of sound pitch was modeled as exponential decay:

$$A = A_0 e^{-t/\tau} \quad (1)$$

Where A0 = 32,767 and $\tau = 0.0003$ where arbitrary values chosen for yhe audibility. To represent the expression level by the pitch level (T), we took an inverse of the average expression value scaled between an inverse of the minimum (MIN) and the maximum (MAX) average value over the three age groups for a given category and mapped on the interval between l = 5 and u = 40:

$$T = l + (u - l)\left(\frac{1}{AV} - \frac{1}{MAX}\right) / \left(\frac{1}{MIN} - \frac{1}{MAX}\right) \quad (2)$$

The ratio between average and SEM was used to generate a sinusoidal pulsing modulation sound with the amplitude AV/SEM:

$$A = A_0 e^{-t/\tau} * \sin(2\pi t f)\left(\frac{AV}{SEM}\right) \quad (3)$$

Where f was typically set to 2000.

These data can be accessed via: https://data.mendeley.com/datasets/22t56fbd6t/draft?a=4b98519d-dfb4−4fe0-a1b0-b4e75b360be6

In addition a musical fingerprint representing each age was created. The reproductive stage was considered as a baseline and corresponds to the unmodified melody of 'Twinkle twinkle little star' played in a C major scale.

To 'hear' the change in the expression level of the 26 selected genes in the prepubertal and menopausal stage the same melody was modified as follows. First, we checked if the protein level was changed by comparing it to the average values at the reproductive stage. If the average value was greater or smaller than SEM, the protein level was assigned as changed. This change was then transformed into a shift in the pitch frequency. The frequency shift was calculated as a fraction fr of the frequency interval to the next (previous) note on the chromatic scale (a halve tone) depending on if the gene expression was higher (lower) compared to the reproductive stage. The fraction fr was obtained as $Repro_{av}/Prepub_{av}$ ($Prepub_{av}/Repro_{av}$) when the protein level was higher (lower) than at the reproductive stage. Thus, for example, a two-fold change in the protein level corresponds to a halve tone pitch change. The data sonification Matlab code can be accessed at the GitHub page: https://github.com/inatamara/Sonificator.

Immunofluorescence and tissue clearing

For validation and localization of ECM biomarkers detected by MS, we used a technique we developed, tailored for 3D immunofluorescence of intact human ovarian ECM of few hundreds of microns (thickness of ovarian cortex) to observe targeted proteins in their inherent 3D configuration and distribution. The workflow is subdivided into five main steps: (1) permeabilization; (2) autofluorescence quenching; (3) non-specific reaction blocking; (4) immunofluorescence labeling; (5) clearing; (6) refractive index balance. At all steps, samples were protected from light.

The permeabilization step consists of washing fixed ovarian tissues (previously kept in 70% ethanol) in PBS for 3 h at RT. Fresh PBS was renewed each hour. The samples were then transferred to a new solution composed of 0.2% Triton-x100 in PBS for 2 h at RT followed by another incubation in 0.2% Triton-x100 and 20% DMSO in PBS overnight at 37° C. Samples were then rinsed in 0.2% Triton-x100 prepared in PBS for 1 h at RT. All these steps were carried out under radial agitation. Autofluorescence quenching was achieved through sample incubation in 1 mg/mL sodium borohydride dissolved in PBS, overnight at RT, and under agitation. The samples were then rinsed in PBS for 90 min with solution renewal every 30 min at RT and under radial agitation. To block non-specific antibody binding, the samples were incubated in 10% fetal bovine serum (FBS), 1% bovine serum albumin (BSA), 1% Triton-x100, and 0.2% Azide at 4°C for 2 days, under radial agitation. After these steps, the samples were ready for antibody labeling. One of the hurdles of conducting immunofluorescence on thick tissue samples is the limited diffusion of antibodies, especially in fibrous samples, such as human ovarian tissue. Therefore, antibodies were resuspended in 10X diluted blocking solution to achieve the required concentration (Table 1) with 500 μL final volume and

were transferred to 1 mL syringes (Baxter Inc, McGaw Park, IL, USA), after hermetically sealing the tips. The samples were subsequently placed into the syringes, and the syringe plunger was put in place. To ensure constant pressure during incubation, the syringes were then packed inside slide staining jars. Incubation with primary antibodies was carried at 4°C under rocking agitation for 5 days under pressure (in syringes). Samples are then transferred to Petri dishes and washed for 2 days in 3% NaCl, 0.2% Triton-x100, and PBS at 4°C under rocking agitation. Like primary antibodies, secondary antibody incubation was carried under pressure at 4°C under rocking agitation, but for only 3 days, followed by a washing step. Nuclear staining was then conducted under pressure in 500x diluted Hoechst in PBS, overnight at 4°C under rocking agitation, and rinsed after in PBS for 3 days at 4°C, under orbital agitation.

Following immunofluorescence, the samples were placed in a 96-well plate and incubated in 100μL RapiClear 1.49 solution (Sunjin Lab, Hsinchu City, Taiwan) at 37°C overnight to achieve transparency. The samples were then kept at 4°C in our in-home developed POTATO (Preservation Of Transparency And Tissue Observation) imaging medium composed of 39% antipyrine, 26% nicotinamide in distilled water, to balance their refractive index (RI) until the day of their analysis.

3D imaging and rendering

With a RI equal to 1.48, the POTATO solution preserves the transparency of ovarian samples perfectly, limits light scattering, offers a cost-effective alternative to expensive commercial solutions, as it is also compatible with most 20X objectives of light-sheet microscopes such as the one we used, a 20x1.0 Clr Plan Neofluar (WD 5.6 mm). On the day of acquisition on Lightsheet.z1 LSFM (Zeiss Inc, Germany), samples were embedded in 1% of low melting agar and pumped in 2.5 mm-diameter capillaries as described by the manufacturer. Cross-linked agar capillaries are then transferred to the imaging chamber filled with POTATO solution and kept at least one hour at RT for RI matching of all imaging system components (sample-media-lens). RI-matched samples were acquired with 408 nm, 488 nm, and 660 nm lasers.

Z stack images (optical slices) were pre-processed and normalized using Zen (black edition) (Zeiss). Video animations were achieved through Arivis 4D (Rivis AG, Rostock, Germany).

For the quantification of positive staining in 3D, we used a macro based on the color threshold tool on Fiji program to report the percentage of the area of green or red pixels by the area of the whole region of interest.

Data availability

The mass spectrometry proteomics data have been deposited to the ProteomeXchange Consortium via the PRIDE [94] partner repository with the dataset identifier PXD (Username: reviewer_pxd025940@ebi.ac.uk; Password: 0K9w3nwz).

All supplementary data can be accessed via the Mendeley depository: https://data.mendeley.com/datasets/22t56fbd6t/draft?a=4b98519d-dfb4−4fe0-a1b0-b4e75b360be6

The data sonification Matlab code can be accessed at the GitHub page: https://github.com/inatamara/Sonificator.

Received 18 October 2021;
Received in revised form 4 March 2022;
Accepted 20 March 2022
Available online 25 March 2022

Keywords:
ECM;
Matrisome;
Fertility;
Oncofertility;
Human ovary;
Follicle;
Proteomics;
TMT;
Data sonification;
Clearing

References

[1] K.A. Piez, History of extracellular matrix: a personal view, Matrix Biol. J. Int. Soc. Matrix Biol. 16 (3) (1997) 85–92.
[2] P. Klemperer, The significance of the intermediate substances of the connective tissue in human disease, Harvey Lect. 49 (1953) 100–123.
[3] U. Rokitansky-Tilscher, Carl Freiherr von Rokitansky's Manual and Rudolf Virchow's criticism: the controversial subject of Rokitansky's doctrine of crases and dyscrases and the groundwork for modern humoral pathology, Wien. Med. Wochenschr. 170 (11) (2020) 284–289.
[4] D. Ribatti, An historical note on the cell theory, Exp. Cell Res. 364 (1) (2018) 1–4.
[5] A. Lopata, History of the egg in embryology, J. Mamm. Ova Res. (1) (2009) 2–9 8.
[6] H.M. Brown, K.R. Dunning, R.L. Robker, M. Pritchard, D.L. Russell, Requirement for ADAMTS-1 in extracellular matrix remodeling during ovarian folliculogenesis and lymphangiogenesis, Dev. Biol. 300 (2) (2006) 699–709.
[7] C. Philippart, R. Masciangelo, A. Camboni, J. Donnez, M.M. Dolmans, Basal lamina characterization in frozen-thawed and long-term grafted human prepubertal ovarian tissue, Reprod. Biomed. Online 42 (5) (2021) 859–869.
[8] H.F. Irving-Rodgers, K. Hummitzsch, L.S. Murdiyarso, W.M. Bonner, Y. Sado, Y. Ninomiya, J.R. Couchman,

L.M. Sorokin, R.J. Rodgers, Dynamics of extracellular matrix in ovarian follicles and corpora lutea of mice, Cell Tissue Res. 339 (3) (2010) 613–624.
[9] R. Jiménez, Ovarian organogenesis in mammals: mice cannot tell Us everything, Sex. Dev. 3 (6) (2009) 291–301.
[10] E. Ouni, S.P.d. Ruys, M.M. Dolmans, G. Herinckx, D. Vertommen, C.A. Amorim, Divide-and-conquer matrisome protein (DC-MaP) strategy: an MS-friendly approach to proteomic matrisome characterization, Int J Mol Sci 21 (23) (2020) 9141.
[11] A. Nikitin, S. Egorov, N. Daraselia, I. Mazo, Pathway studio—the analysis and navigation of molecular networks, Bioinformatics 19 (16) (2003) 2155–2157.
[12] C.A. Amorim, P. Asiabi, E. Ouni, J. Vilela, A. Camboni, C. Maria Costanza, P.P. Grynberg Michael, Chapter 30: transplantation of isolated follicles and the engineered ovary. Female and male fertility preservation, Female and Male Fertility Preservation, Springer, 2021.
[13] M. Ruehl, U. Erben, D. Schuppan, C. Wagner, A. Zeller, C. Freise, H. Al-Hasani, M. Loesekann, M. Notter, B.M. Wittig, M. Zeitz, W. Dieterich, R. Somasundaram, The elongated first fibronectin type III domain of collagen XIV is an inducer of quiescence and differentiation in fibroblasts and preadipocytes, J. Biol. Chem. 280 (46) (2005) 38537–38543.
[14] T.W. Kelsey, P. Wright, S.M. Nelson, R.A. Anderson, W.H. Wallace, A validated model of serum anti-mullerian hormone from conception to menopause, PLoS One 6 (7) (2011) e22024.
[15] K. Ozegowska, A. Bogacz, J. Bartkowiak-Wieczorek, A. Seremak-Mrozikiewicz, L. Pawelczyk, Association between the angiotensin converting enzyme gene insertion/deletion polymorphism and metabolic disturbances in women with polycystic ovary syndrome, Mol. Med. Rep. 14 (6) (2016) 5401–5407.
[16] Y. Yoshimura, The ovarian renin-angiotensin system in reproductive physiology, Front. Neuroendocrinol. 18 (3) (1997) 247–291.
[17] L. Cuiling, Y. Wei, H. Zhaoyuan, L. Yixun, Granulosa cell proliferation differentiation and its role in follicular development, Chin. Sci. Bull. 50 (23) (2005) 2665.
[18] C. Zeng, R. Yan, G. Yang, S. Xiang, F. Zhao, Hedgehog signaling activation required for glypican-6-mediated regulation of invasion, migration, and epithelial-mesenchymal transition of gastric cancer cells, Biosci. Rep. 40 (6) (2020).
[19] H.F. Irving-Rodgers, R.J. Rodgers, Extracellular matrix in ovarian follicular development and disease, Cell Tissue Res. 322 (1) (2005) 89–98.
[20] A.G. Marneros, B.R. Olsen, Physiological role of collagen XVIII and endostatin, FASEB J. 19 (7) (2005) 716–728.
[21] K. Klement, C. Melle, U. Murzik, S. Diekmann, J. Norgauer, P. Hemmerich, Accumulation of annexin A5 at the nuclear envelope is a biomarker of cellular aging, Mech. Ageing Dev. 133 (7) (2012) 508–522.
[22] M. Mela, W. Smeeton, S.E. Davies, E. Miranda, C. Scarpini, N. Coleman, G.J.M. Alexander, The alpha-1 antitrypsin polymer load correlates with hepatocyte senescence, fibrosis stage and liver-related mortality, Chronic Obstr. Pulm. Dis. 7 (3) (2020) 151–162.
[23] H. Hasan, S.H. Park, C. Auger, E. Belcastro, K. Matsushita, B. Marchandot, H.H. Lee, A.W. Qureshi, G. Kauffenstein, P. Ohlmann, V.B. Schini-Kerth, L. Jesel, O. Morel, Thrombin induces angiotensin II-mediated senescence in atrial endothelial cells: impact on pro-remodeling patterns, J. Clin. Med. 8 (10) (2019).
[24] H.F. Irving-Rodgers, K.D. Catanzariti, W.J. Aspden, M.J. D'Occhio, R.J. Rodgers, Remodeling of extracellular matrix at ovulation of the bovine ovarian follicle, Mol. Reprod. Dev. 73 (10) (2006) 1292–1302.
[25] K. Iba, N. Hatakeyama, T. Kojima, M. Murata, T. Matsumura, U.M. Wewer, T. Wada, N. Sawada, T. Yamashita, Impaired cutaneous wound healing in mice lacking tetranectin, Wound Repair Regen. 17 (1) (2009) 108–112.
[26] L. Parente, E. Solito, Annexin 1: more than an anti-phospholipase protein, Inflamm. Res. 53 (4) (2004) 125–132.
[27] Z. Lu, D. Cheng, J. Yin, R. Wu, G. Zhang, Q. Zhao, N. Wang, F. Wang, M. Liang, Antithrombin III protects against contrast-induced nephropathy, EBioMedicine 17 (2017) 101–107.
[28] S.M. Briley, S. Jasti, J.M. McCracken, J.E. Hornick, B. Fegley, M.T. Pritchard, F.E. Duncan, Reproductive age-associated fibrosis in the stroma of the mammalian ovary, Reproduction 152 (3) (2016) 245–260.
[29] S. Chen, D.E. Birk, The regulatory roles of small leucine-rich proteoglycans in extracellular matrix assembly, FEBS J. 280 (10) (2013) 2120–2137.
[30] K. Musselmann, B. Kane, B. Alexandrou, J.R. Hassell, Stimulation of collagen synthesis by insulin and proteoglycan accumulation by ascorbate in bovine keratocytes *in vitro*, Invest. Ophthalmol. Vis. Sci. 47 (12) (2006) 5260–5266.
[31] P. Rappu, A.M. Salo, J. Myllyharju, J. Heino, Role of prolyl hydroxylation in the molecular interactions of collagens, Essays Biochem. 63 (3) (2019) 325–335.
[32] R.C. Wilson, A. Shenhav, M. Straccia, J.D. Cohen, The eighty five percent rule for optimal learning, Nat. Commun. 10 (1) (2019) 4646.
[33] R.A. Anderson, M. McLaughlin, W.H. Wallace, D.F. Albertini, E.E. Telfer, The immature human ovary shows loss of abnormal follicles and increasing follicle developmental competence through childhood and adolescence, Hum. Reprod. 29 (1) (2014) 97–106.
[34] J. Zhou, X. Peng, S. Mei, Autophagy in ovarian follicular development and atresia, Int. J. Biol. Sci. 15 (4) (2019) 726–737.
[35] I.M. Sheldon, J.J. Bromfield, Innate immunity in the human endometrium and ovary, Am. J. Reprod. Immunol. 66 (Suppl 1) (2011) 63–71.
[36] D.F. Boyd, P.G. Thomas, Towards integrating extracellular matrix and immunological pathways, Cytokine 98 (2017) 79–86.
[37] X. Jiao, H. Ke, Y. Qin, Z.J. Chen, Molecular genetics of premature ovarian insufficiency, Trends Endocrinol. Metab. 29 (11) (2018) 795–807.
[38] H. Zou, C. Wen, Z. Peng, Y. Shao, L. Hu, S. Li, C. Li, H.H. Zhou, P4HB and PDIA3 are associated with tumor progression and therapeutic outcome of diffuse gliomas, Oncol. Rep. 39 (2) (2018) 501–510.
[39] J.H. Lee, E.J. Kwon, D.H. Kim, Calumenin has a role in the alleviation of ER stress in neonatal rat cardiomyocytes, Biochem. Biophys. Res. Commun. 439 (3) (2013) 327–332.
[40] R. Philippe, O. Mignen, Measuring calumenin impact on ER-calcium depletion using transient calumenin overexpression and silencing, Methods Mol. Biol. 1929 (2019) 539–550.
[41] M. Fu, L. Li, T. Albrecht, J.D. Johnson, L.D. Kojic, I.R. Nabi, Autocrine motility factor/phosphoglucose isomerase regulates ER stress and cell death through control of ER calcium release, Cell Death Differ. 18 (6) (2011) 1057–1070.
[42] Y. Lim, D. Lee, K. Kalichamy, S.E. Hong, M. Michalak, J. Ahnn, D.H. Kim, S.K. Lee, Sumoylation regulates ER stress response by modulating calreticulin gene expression

in XBP-1-dependent mode in caenorhabditis elegans, Int. J. Biochem. Cell Biol. 53 (2014) 399–408.
[43] K. Kawamura, Y. Cheng, N. Suzuki, M. Deguchi, Y. Sato, S. Takae, C.H. Ho, N. Kawamura, M. Tamura, S. Hashimoto, Y. Sugishita, Y. Morimoto, Y. Hosoi, N. Yoshioka, B. Ishizuka, A.J. Hsueh, Hippo signaling disruption and Akt stimulation of ovarian follicles for infertility treatment, Proc. Natl. Acad. Sci. U. S. A. 110 (43) (2013) 17474–17479.
[44] J. Gatliff, D. East, J. Crosby, R. Abeti, R. Harvey, W. Craigen, P. Parker, M. Campanella, TSPO interacts with VDAC1 and triggers a ROS-mediated inhibition of mitochondrial quality control, Autophagy 10 (12) (2014) 2279–2296.
[45] I. Koren, E. Reem, A. Kimchi, DAP1, a novel substrate of mTOR, negatively regulates autophagy, Curr. Biol. 20 (12) (2010) 1093–1098.
[46] E.G. Pamer, Cellular immunity to intracellular bacteria, Curr. Opin. Immunol. 5 (4) (1993) 492–496.
[47] D.M. Duffy, C. Ko, M. Jo, M. Brannstrom, T.E. Curry, Ovulation: parallels with inflammatory processes, Endocr. Rev. 40 (2) (2019) 369–416.
[48] R.G. Khalifah, J.W. Baynes, B.G. Hudson, Amadorins: novel post-Amadori inhibitors of advanced glycation reactions, Biochem. Biophys. Res. Commun. 257 (2) (1999) 251–258.
[49] C.Y. Ewald, The matrisome during aging and longevity: a systems-level approach toward defining matreotypes promoting healthy aging, Gerontology 66 (3) (2020) 266–274.
[50] E. Ouni, A. Peaucelle, K.T. Haas, O. Van Kerk, M.M. Dolmans, T. Tuuri, M. Otala, D. Vertommen, C.A. Amorim, A multi-scale readout of the microarchitecture, topography and mechanics of human ovary from prepuberty to menopause for the next generation of tissue engineered ovary and clinical diagnosis, Nat. Commun. (2021) (under review).
[51] J.L. Zhu, Y.Q. Cai, S.L. Long, Z. Chen, Z.C. Mo, The role of advanced glycation end products in human infertility, Life Sci. 255 (2020) 117830.
[52] C.N. Cordeiro, M.S. Christianson, J.H. Selter, J.H. Segars, *In vitro* activation: a possible new frontier for treatment of primary ovarian insufficiency, Reprod. Sci. 23 (4) (2016) 429–438 (Thousand Oaks, Calif.).
[53] Y. Cheng, Y. Feng, L. Jansson, Y. Sato, M. Deguchi, K. Kawamura, A.J. Hsueh, Actin polymerization-enhancing drugs promote ovarian follicle growth mediated by the hippo signaling effector YAP, FASEB J. 29 (6) (2015) 2423–2430.
[54] Y. Cheng, J. Kim, X.X. Li, A.J. Hsueh, Promotion of ovarian follicle growth following mTOR activation: synergistic effects of AKT stimulators, PLoS One 10 (2) (2015) e0117769.
[55] Y. Tong, F. Li, Y. Lu, Y. Cao, J. Gao, J. Liu, Rapamycin-sensitive mTORC1 signaling is involved in physiological primordial follicle activation in mouse ovary, Mol. Reprod. Dev. 80 (12) (2013) 1018–1034.
[56] L. Li, S.Y. Ji, J.L. Yang, X.X. Li, J. Zhang, Y. Zhang, Z.Y. Hu, Y.X. Liu, Wnt/β-catenin signaling regulates follicular development by modulating the expression of Foxo3a signaling components, Mol. Cell. Endocrinol. 382 (2) (2014) 915–925.
[57] A.D. Stapp, B.I. Gomez, C.A. Gifford, D.M. Hallford, J.A. Hernandez Gifford, Canonical WNT signaling inhibits follicle stimulating hormone mediated steroidogenesis in primary cultures of rat granulosa cells, PLoS One 9 (1) (2014) e86432.
[58] D. Herr, I. Bekes, C. Wulff, Local renin-angiotensin system in the reproductive system, Front. Endocrinol. 4 (2013) 150 (Lausanne).
[59] H. Yan, J. Wen, T. Zhang, W. Zheng, M. He, K. Huang, Q. Guo, Q. Chen, Y. Yang, G. Deng, J. Xu, Z. Wei, H. Zhang, G. Xia, C. Wang, Oocyte-derived E-cadherin acts as a multiple functional factor maintaining the primordial follicle pool in mice, Cell Death Dis. 10 (3) (2019) 160.
[60] E. Ouni, D. Vertommen, M.C. Chiti, M.M. Dolmans, C.A. Amorim, A draft map of the human ovarian proteome for tissue engineering and clinical applications, Mol. Cell. Proteom. 18 (Suppl 1) (2019) S159–S173.
[61] T.K. Woodruff, L.D. Shea, The role of the extracellular matrix in ovarian follicle development, Reprod. Sci. 14 (8 Suppl) (2007) 6–10 (Thousand Oaks, Calif.).
[62] C.B. Berkholtz, B.E. Lai, T.K. Woodruff, L.D. Shea, Distribution of extracellular matrix proteins type I collagen, type IV collagen, fibronectin, and laminin in mouse folliculogenesis, Histochem. Cell Biol. 126 (5) (2006) 583–592.
[63] R. Abir, P. Roizman, B. Fisch, S. Nitke, E. Okon, R. Orvieto, Z. Ben Rafael, Pilot study of isolated early human follicles cultured in collagen gels for 24h, Hum. Reprod. 14 (5) (1999) 1299–1301.
[64] R. Abir, B. Fisch, S. Nitke, E. Okon, A. Raz, Z.B Rafael, Morphological study of fully and partially isolated early human follicles, Fertil. Steril. 75 (1) (2001) 141–146.
[65] E. Telfer, C. Torrance, R.G. Gosden, Morphological study of cultured preantral ovarian follicles of mice after transplantation under the kidney capsule, J. Reprod. Fertil. 89 (2) (1990) 565–571.
[66] J. Carroll, D.G. Whittingham, M.J. Wood, Effect of gonadotrophin environment on growth and development of isolated mouse primary ovarian follicles, J. Reprod. Fertil. 93 (1) (1991) 71–79.
[67] S. Itami, K. Yasuda, Y. Yoshida, C. Matsui, S. Hashiura, A. Sakai, S. Tamotsu, Co-culturing of follicles with interstitial cells in collagen gel reproduce follicular development accompanied with theca cell layer formation, Reprod. Biol. Endocrinol. 9 (2011) 159.
[68] M. Cescon, F. Gattazzo, P. Chen, P. Bonaldo, Collagen VI at a glance, J. Cell Sci. 128 (19) (2015) 3525–3531.
[69] S.R. Lamandé, J.F. Bateman, Collagen VI disorders: Insights on form and function in the extracellular matrix and beyond, Matrix Biol. J. Int. Soc. Matrix Biol. 71-72 (2018) 348–367.
[70] T. Neill, A. Kapoor, C. Xie, S. Buraschi, R.V. Iozzo, A functional outside-in signaling network of proteoglycans and matrix molecules regulating autophagy, Matrix Biol. 100-101 (2021) 118–149.
[71] P. Mermillod, R. Dalbiès-Tran, S. Uzbekova, A. Thélie, J.M. Traverso, C. Perreau, P. Papillier, P. Monget, Factors affecting oocyte quality: who is driving the follicle? Reprod. Domest. Anim. 43 (Suppl 2) (2008) 393–400.
[72] E. Ouni, C. Bouzin, M.M. Dolmans, E. Marbaix, S. Pyr Dit Ruys, D. Vertommen, C.A. Amorim, Spatiotemporal changes in mechanical matrisome components of the human ovary from prepuberty to menopause, Hum. Reprod. 35 (6) (2020) 1391–1410.
[73] E.R. Lumbers, K.G. Pringle, Roles of the circulating renin-angiotensin-aldosterone system in human pregnancy, Am. J. Physiol. Regul. Integr. Comp. Physiol. 306 (2) (2014) R91–101.
[74] C.B. Tempfer, R.M. Moreno, A.R. Gregg, Genetic control of fertility and embryonic waste in the mouse: a role for angiotensinogen 1, Biol. Reprod. 62 (2) (2000) 457–462.
[75] S.A. Ye, S. Everman, E.D. Torres Fernandez, D.G. Romero, L.L. Yanes Cardozo, Renal androgen and renin angiotensin

system mRNA expression in polycystic ovary syndrome, FASEB J. 34 (S1) (2020) 1.
[76] J. Filmus, M. Capurro, J. Rast, Glypicans, Genome Biol. 9 (5) (2008) 224.
[77] R.S. Robinson, K.J. Woad, A.J. Hammond, M. Laird, M.G. Hunter, G.E. Mann, Angiogenesis and vascular function in the ovary, Reproduction 138 (6) (2009) 869–881.
[78] D.A. Redmer, L.P. Reynolds, Angiogenesis in the ovary, Rev. Reprod. 1 (3) (1996) 182–192.
[79] C.H. Lin, J. Chen, Z. Zhang, G.V. Johnson, A.J. Cooper, J. Feola, A. Bank, J. Shein, H.J. Ruotsalainen, T.A. Pihlajaniemi, M.S. Goligorsky, Endostatin and transglutaminase 2 are involved in fibrosis of the aging kidney, Kidney Int. 89 (6) (2016) 1281–1292.
[80] L. Montecinos, J.D. Eskew, A. Smith, What is next in this "age" of heme-driven pathology and protection by hemopexin? An update and links with iron, Pharmaceuticals 12 (4) (2019) (Basel).
[81] D. Harman, Aging: a theory based on free radical and radiation chemistry, J. Gerontol. 11 (3) (1956) 298–300.
[82] S. Wang, Y. Zheng, J. Li, Y. Yu, W. Zhang, M. Song, Z. Liu, Z. Min, H. Hu, Y. Jing, X. He, L. Sun, L. Ma, C.R. Esteban, P. Chan, J. Qiao, Q. Zhou, J.C. Izpisua Belmonte, J. Qu, F. Tang, G.H. Liu, Single-cell transcriptomic atlas of primate ovarian aging, Cell 180 (3) (2020) 585–600.e19.
[83] Y. Huang, C. Hu, H. Ye, R. Luo, X. Fu, X. Li, J. Huang, W. Chen, Y. Zheng, Inflamm-aging: a new mechanism affecting premature ovarian insufficiency, J. Immunol. Res. (2019) 8069898 2019.
[84] F. Prattichizzo, L. Micolucci, M. Cricca, S. De Carolis, E. Mensà, A. Ceriello, A.D. Procopio, M. Bonafè, F. Olivieri, Exosome-based immunomodulation during aging: a nano-perspective on inflamm-aging, Mech. Ageing Dev. 168 (2017) 44–53.
[85] N. Thevaranjan, A. Puchta, C. Schulz, A. Naidoo, J.C. Szamosi, C.P. Verschoor, D. Loukov, L.P. Schenck, J. Jury, K.P. Foley, J.D. Schertzer, M.J. Larché, D.J. Davidson, E.F. Verdú, M.G. Surette, D.M.E. Bowdish, Age-associated microbial dysbiosis promotes intestinal permeability, systemic inflammation, and macrophage dysfunction, Cell Host Microbe 21 (4) (2017) 455–466 e4.
[86] A. Salminen, J. Huuskonen, J. Ojala, A. Kauppinen, K. Kaarniranta, T. Suuronen, Activation of innate immunity system during aging: NF-kB signaling is the molecular culprit of inflamm-aging, Ageing Res. Rev. 7 (2) (2008) 83–105.
[87] D. Geroldi, C. Falcone, E. Emanuele, Soluble receptor for advanced glycation end products: from disease marker to potential therapeutic target, Curr. Med. Chem. 13 (17) (2006) 1971–1978.
[88] M. Laszczyńska, A. Brodowska, A. Starczewski, M. Masiuk, J. Brodowski, Human postmenopausal ovary−hormonally inactive fibrous connective tissue or more? Histol. Histopathol. 23 (2) (2008) 219–226.
[89] W.B. Cannon, The Wisdom of the Body, Peter Smith Pub Inc, 1963 Ed edition ed.
[90] N. Ogrinc, P. Saudemont, J. Balog, Y.M. Robin, J.P. Gimeno, Q. Pascal, D. Tierny, Z. Takats, M. Salzet, I. Fournier, Water-assisted laser desorption/ionization mass spectrometry for minimally invasive *in vivo* and real-time surface analysis using spidermass, Nat. Protoc. 14 (11) (2019) 3162–3182.
[91] WHO, World Report on Disability, WHO, 2011.
[92] C.A. Amorim, A. Van Langendonckt, A. David, M.M. Dolmans, J. Donnez, Survival of human pre-antral follicles after cryopreservation of ovarian tissue, follicular isolation and *in vitro* culture in a calcium alginate matrix, Hum. Reprod. 24 (1) (2009) 92–99.
[93] S. Novichkova, S. Egorov, N. Daraselia, MedScan, a natural language processing engine for MEDLINE abstracts, Bioinformatics 19 (13) (2003) 1699–1706.
[94] Y. Perez-Riverol, A. Csordas, J. Bai, M. Bernal-Llinares, S. Hewapathirana, D.J. Kundu, A. Inuganti, J. Griss, G. Mayer, M. Eisenacher, E. Perez, J. Uszkoreit, J. Pfeuffer, T. Sachsenberg, S. Yilmaz, S. Tiwary, J. Cox, E. Audain, M. Walzer, A.F. Jarnuczak, T. Ternent, A. Brazma, J.A. Vizcaino, The PRIDE database and related tools and resources in 2019: improving support for quantification data, Nucleic Acids Res. 47 (D1) (2019) D442–D450.